Digital Comprehensive Summaries of Uppsala Dissertations
from the Faculty of Science and Technology 2485

Industrial robot as main equipment for testing and production of Wave Energy Converters

DANA SALAR

ACTA UNIVERSITATIS
UPSALIENSIS
2025

ISSN 1651-6214
ISBN 978-91-513-2337-4
urn:nbn:se:uu:diva-544285

UPPSALA
UNIVERSITET

Dissertation presented at Uppsala University to be publicly examined in Polhem, Lägerhyddsvägen 1, 75237 Uppsala, Uppsala, Monday, 10 February 2025 at 09:15 for the degree of Doctor of Philosophy. The examination will be conducted in English. Faculty examiner: Dr Jonas Öhr (ABB Crane Systems, Sweden).

Abstract

Salar, D. 2025. Industrial robot as main equipment for testing and production of Wave Energy Converters. *Digital Comprehensive Summaries of Uppsala Dissertations from the Faculty of Science and Technology* 2485. 78 pp. Uppsala: Acta Universitatis Upsaliensis. ISBN 978-91-513-2337-4.

Since 2001, research and development on the conversion of ocean wave energy into electricity has been conducted at the Division of Electricity at Uppsala University. Different Wave Energy Converter (WEC) technologies has been developed, such as the point-absorber linear Uppsala University WEC (UU-WEC) and the Low-RPM Torque Converter WEC (LRTC-WEC).

This thesis focuses primarily on the development of a robotized dry test rig, to facilitate assessment of different WEC technologies in house. An existing industrial six degrees of freedom robot system is used to emulate buoy movement on the sea surface, with regard to the impact of hydrodynamic forces in real time. Two different methods for integrating a hydrodynamic model to the robot controller are presented: the force control and the position control methods. Both methods are evaluated and validated across various regular and irregular wave climates, as well as for different theoretical buoy shapes.

The secondary focus in this thesis is the development of robotized production methods for the UU-WEC. The surface mounting of Neodymium Iron Boron (Nd2Fe14B) magnets and the cutting of rubber discs are investigated, resulting in viable solutions that include development and validation of robot tooling and robot cell proposals.

A smaller segment of the thesis examines the use of robotics in teaching a course for bachelor engineering students. At the outbreak of the COVID-19 pandemic a challenging task was imposed: a swift shift to online distant education. A major task was to replace physical lab exercises with video recordings, detailed instructions and simulated laboratory environments. The results indicated that the upgraded online education successfully meet the course objectives.

The final part of the thesis investigates the use of WECs for powering a desalination plant. Desalination presents a viable solution for islands or coastal regions deficient in freshwater resources, but is also an energy intensive process. Practical experiment evaluated the possibility of utilizing the UU-WEC as power source for desalination plants.

Keywords: Dry test rig, Industrial robotics, Manufacturing automation, Large-scale production, Linear generator, Wave energy converter, Engineering education, Desalination

Dana Salar, Department of Electrical Engineering, Electricity, Box 65, Uppsala University, SE-751 03 Uppsala, Sweden.

ISSN 1651-6214
ISBN 978-91-513-2337-4
URN urn:nbn:se:uu:diva-544285 (http://urn.kb.se/resolve?urn=urn:nbn:se:uu:diva-544285)

Till Mila och Adam

List of Papers

This thesis is based on the following papers, which are referred to in the text by their Roman numerals.

I. Savin, A., **Salar, D.**, Hultman, E. (2021) Low-RPM Torque Converter (LRTC), *Energies,* vol.14, no.16, 5071.

II. **Salar, D.**, Hultman, E., Savin, A. (2023) The Low-RPM torque converter (LRTC) with integrated direct shaft flywheel. *International Marine Energy Journal*, vol.6, no.1, pp.1–10.

III. Hultman, E., **Salar, D.** (2023) A robotized 6-DOF dry test rig for wave power, *Sustainable Energy Technologies and Assessments,* vol.59, 103393.

IV. **Salar, D.**, Hultman, E. (2023) Demonstrating real-time hydrodynamic motion response in force control for regular waves in a robotized dry test rig with a point-absorber WEC, *Proceedings of the 15^{ht} European Wave and Tidal Energy Conference,* Bilbao, Spain.

V. **Salar, D.**, Hultman, E. (2024) Evaluating position control for real-time hydrodynamic motion response in a robotized dry test rig with a point-absorber WEC. *Proceedings of the 43rd International Conference on Ocean, Offshore and Arctic Engineering,* Singapore.

VI. **Salar, D.**, Dupuis, A., Hultman, E. (2024) Emulating wave energy converter operation in irregular waves using a robotized dry test rig. *Unpublished Manuscript, December 2024*

VII. Hultman, E., Ekergård, B., Kamf, T., **Salar, D.**, Leijon, M. (2014) Preparing the Uppsala University wave energy converter generator for large-scale production. *Proceedings of the 5th International Conference on Ocean Energy*, Halifax, Canada.

VIII. Hultman, E., **Salar, D.** and Leijon, M. (2014) Robotized surface mounting of permanent magnets. *MDPI Machines*; vol.2, pp.219-232.

IX. Hultman, E., **Salar, D.**, Åberg, E., Leijon, M. (2016) Robotized manufacturing of rubber components for commercialization of the Uppsala University wave energy converter concept. *Proceedings of the 2nd International Conference on Offshore Renewable Energy,* Glasgow, UK.

X. Hultman, E., **Salar**, D. (2022) Learnings from the rapid online transition of a real-world project task-based engineering course, *Proceedings of the international Frontiers in Education Conference*, Uppsala, Sweden.

XI. Leijon, J., **Salar, D.**, Engström, J., Leijon, M., Boström, C. (2020) Variable renewable energy sources for powering reverse osmosis desalination, with a case study of wave powered desalination for Kilifi, Kenya, *Desalination*, vol.494, 114669.

Reprints were made with permission from the respective publishers.

Contents

List of Symbols

Symbol	Unit	Description
A_m	kg	added mass
A_s	m	the transversal area off the buoy
$B(\omega)$, $B_c(\omega)$	Ns/m	the buoy's radiation damping coefficient
D	m	the buoy diameter
d	m	the draft defined as the height of the buoy underwater at equilibrium
F_{exc}	N	the excitation force
F_h	N	the hydrostatic force
F_{hyd}	N	the total hydrodynamic force acting on the buoy
F_{line}	N	the line force
F_{nr}	N	the Froude number
F_{pto}	N	the PTO force
F_r	N	the radiation force
F_{ref1}	N	the reference force for one-body model
F_{ref2}	N	the reference force for two-body model
$F_{standstill}$	N	the line force at the standstill
F_w	N	the WECs weight force
$F_{w,b}$	N	the buoys weight force
g	m/s^2	the acceleration of gravity
H_s	m	the significant wave height
$\widehat{\boldsymbol{K}}$	-	the unit vector positive in the upward direction
l	m	the characteristic dimension of the WEC
m_b	kg	the mass of the buoy
m_{wec}	kg	the mass of the WEC
m_∞	kg	the buoy's added mass at infinite frequency
R	m	the buoy radius
T_p	m	wave period
U	m/s	the relative speed of the WEC body

z, x	m	position
$\dot{z}$, $\dot{x}$	m/s	velocity
$\ddot{z}$, $\ddot{x}$	m/s^2	acceleration
η	m	the wave surface elevation
ρ	kg/m^3	the density
γ_{pto}	Ns/m	the PTO damping coefficient
γ_{rob}	Ns/m	the robot damping coefficient
$\Gamma(\omega)$	N/m	the excitation force amplitude
ω	rad/s	the wave angular frequency

Abbreviations

Abbreviation	Description
AC	Alternating Current
$B_{1,2}$	Buoy one and buoy two
BEM	Boundary Element Method
CAM	Computer-Aided Manufacturing
CNC	Computer Numerical Control
DC	Direct Current
DOF	Degree Of Freedom
DP	Desalination Park
EPDM	Ethylene Propylene Diene Monomer
LRTC	Low-RPM Torque Converter
LPF	Linear Potential Flow
MCS	Monitoring Control System
$Nd_2Fe_{14}B$	Neodymium Iron Boron
NRMSE	Normalized Root Mean Square Error
PM	Permanent Magnet
PTO	Power Take-Off
RES	Renewable Energy Sources
RO	Reverse Osmosis
SC_{1-4}	Study Case one to four
UU-WEC	Uppsala University wave energy converter concept.
$W_{1,2}$	Wave one and wave two
WAMIT	Wave Analysis developed at the Massachusetts Institute of Technology
WEC	Wave Energy Converter

1 Introduction

Energy consumption and sources are central to the global discourse on addressing environmental issues and the need for eco-friendly solutions. The harmful effects of fossil-based energy sources on the environment show the increasing need to switch to sustainable and renewable energy sources. The use of renewable energy represents considerable advantages for the environment [1]. Various techniques exist to capture energy from natural sources including solar, wind and ocean waves. Ocean waves are well known as a very promising source of energy. The abundant presence of ocean waves and significant energy density, regardless of time of the day or season, results in a high utilization coefficient [2]. With the use of Wave Energy Converters (WECs), achieving sustainable and cost-effective electricity generation remains a challenging goal for both academics and energy providers [3-5].

For more than 20 years, research at the Division of Electricity has focused on renewable energy conversion. About 43 PhDs have defended their thesis on different aspects of wave power [6-49].

A Power Take-Off (PTO) mechanism is essential in the context of WECs. It converts the mechanical energy harnessed from ocean waves into useful electrical energy. Efficient PTO systems are crucial for enhancing the effectiveness and reliability of wave energy conversion.

Global progress drives the continuous evolution of new WEC concepts. Key focus areas include production, testing, and evaluation for each WEC design. Early testing and evaluation is essential but often time-intensive. Once a full-scale design is established, the next step is to fabricate the WEC model using a high-efficiency and cost-effective manufacturing process.

1.1 UU-WEC

A well-known innovation from the Division of Electricity is the Uppsala University WEC (UU-WEC), a linear direct drive generator integrated with a point absorber buoy (see Figure 1) developed within the Lysekil project and tested on Sweden's west coast [50-52]. The modular UU-WEC linear generator consists of two main components: a fixed part and a moving part. The stator package, consisting of coil windings, is securely enclosed within a cylindrical casing. In the centre of the stator packages, a 3-meter-long magnet lump (translator) is positioned, with rails and wheels serving as a linear guiding. A wired connection links the translator to a buoy located on the surface of the sea.

As the buoy rises and falls with the waves, the attached translator-magnet assembly moves up and down through the stator coils, inducing current in the coils. This movement harnesses the ocean's kinetic energy for electricity generation.

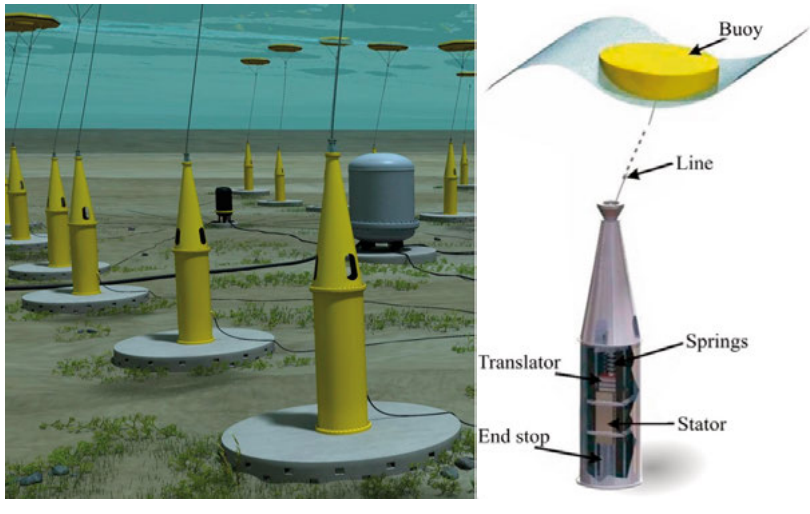

Figure 1. The UU-WEC concept, developed at Uppsala University [Paper XI]

1.2 LRTC-WEC

A few years ago, a new concept for renewable energy, the Low-RPM Torque Converter WEC (LRTC-WEC), was introduced at the Division of Electricity [Paper I, II]. The LRTC-WEC operates as a rotating electrical generator that transforms the motion of ocean waves into mechanical energy to generate electricity. Like the UU-WEC, it is installed on the seabed and connected to a buoy on sea surface via a wire (see Figure 2).

The LRTC-WEC design consists of two identical three-phase rotating generators connected by a specialized drum. The drum houses two ball bearings that allow each generator to rotate in opposite directions. A spring connected to the drum applies a retracting force, creating tension in a wire wound around it. This wire connects to the buoy on the sea surface. As waves cause the buoy to rise, it pulls one of the generators around. On the contrary, when the wave falls, the spring pulls the drum back, activating the second generator in the opposite direction. With continuous wave motion, both generators spin continuously in opposite directions to each other.

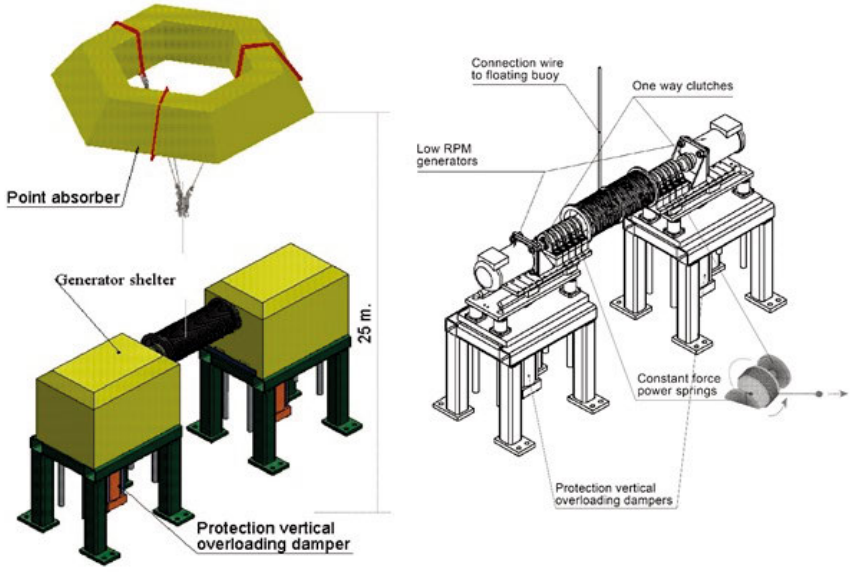

Figure 2. The UU LRTC-WEC concept [Paper I]

1.3 Research aim and thesis outline

This thesis covers several aspects related to the WEC. The thesis is divided into four parts.

- The main goal is to develop a robotized dry test rig for assessment and evaluation of diverse point absorber WEC technologies.
- The secondary purpose is to develop automation solutions for two production steps of the UU-WEC that are classified as risky, tiring and time-consuming work.
- Transform a campus-based, experimental lab exercise into a completely online distance learning format.
- Contributing to investigating the possibility of using the UU-WEC to power a desalination plant.

The first part of the thesis, covering Papers I–VI, focuses on establishing the use of a six Degrees Of Freedom (6-DOF) industrial robot as a dry test rig for assessing various point absorber WEC designs.

The second part, including Papers VII–IX, investigates automated manufacturing techniques for the UU-WEC using a 6-DOF industrial robot.

As part of doctoral responsibilities, this work includes participation in teaching and course material development. Paper X presents findings and developments related to pedagogical strategies for distance learning.

Beyond these projects, the research also explores measurement technologies for WEC generators. Paper XI specifically investigates the potential of WECs to power a desalination unit for converting saltwater into freshwater.

2 Method

This research builds upon previously discussed topics over an extended period. Experiments were essential for the work in all parts of the thesis. The primary software that significantly aided parallel tasks during the actual experiment is RobotStudio from ABB.

RobotStudio is an advanced simulation and offline programming software that allows users to design, simulate, and optimize robotic systems prior to their implementation in practical applications. This technology offers a virtual environment for users to develop and evaluate robotic algorithms, guaranteeing their efficiency and accuracy.

This thesis was partially created with grammatical and phrasing assistance from the generative AI tool Quillbot. Upon generating draft language, I reviewed, edited, and refined the text to my own liking and retain full responsibility for the content presented in this publication.

- In the initial part, an existing 6-DOF industrial robot manipulator was thoroughly investigated and developed as a test rig; details of this work are documented in Paper I–VI. The primary objective was to develop a new type of dry test rig for testing and assessing WEC technologies and provide additional opportunities for evaluation.
- In part two, the focus was on robotized manufacturing technologies for the UU-WEC, targeting key components essential for efficient robotic production. The goal was to minimize repetitive and strenuous manual tasks while developing a streamlined, adaptable manufacturing system. Detailed findings are available in Paper VII–IX.
- In part three, a fully campus-based, hands-on robotics and automation course was transformed into a completely online distance course due to the COVID-19 pandemic. Detailed findings are available in Paper X.
- In part four, the potential of utilizing renewable energy sources, such as WECs, to power a desalination plant was investigated. Detailed findings are available in Paper XI.

2.1 Robot dry test rig

The development of the robot dry test rig utilized a multi-phase methodology, with each phase facing different technical challenges. Due to the complexity of the concept, it has been crucial that the process has to a large extent included experimental development and assessment.

Stage one: In this preliminary phase, the implementation and exploration of passive robotized testing were aimed at assessing the LRTC-WEC concept, without using force feedback to the robot. A force measurement instrument was designed to quantify the tension force in the wire in one direction. The data collected was transmitted to a PC, where a specialized LabView module processed the sensor data and translated it into force measurements in Newton. Furthermore, a measurement technique was developed to measure the voltage and current generated by the LRTC-PTO, with all data being analyzed using LabVIEW [Paper I–II].

Stage two: This phase entailed assessing the system's operational limitations and verifying the complete test rig configuration under small regular wave movements. Two active control strategies—force control and position control—were evaluated under these conditions to assess their effectiveness [Paper III].

Stage three: During this phase, the precision of the force control method was assessed. The error associated with the system was analyzed by examining the robot's motion response and the radiation force implementation. A fast motion response occurs when the damping is reduced towards zero, which was not feasible as it resulted in the system becoming unbalanced. To obtain stable measurements of speed and acceleration, these variables were filtered using Low-Pass (LP) filtering. This technique, however, resulted in a control delay, which was noted for subsequent research [Paper IV].

Stage four: During this phase, position control was executed, and the system's response to various control lag conditions was assessed. To enhance response time, the trade-off between reducing control lag and the potential increase in deviation and overshoot was evaluated for a suggested updated control method [Paper V].

Final stage: In the concluding validation phase, the hydrodynamic model was enhanced to accommodate irregular wave patterns. The updated model implementation was validated through numerical simulations in four case studies, incorporating an additional buoy geometry. Considering the robot's computational constraints, the suitable history time for the model computations was also assessed, and the robot test rig was evaluated against a wave tank experiment [Paper VI].

2.2 Robotized production

The work on robotized production focused on two steps of the UU-WEC manufacturing: the assembly of surface-mounted Neodymium Iron Boron ($Nd_2Fe_{14}B$) magnets, which constitute the moving part of the UU-WEC; and cutting rubber discs that are used to prevent the wire from snapping between the PTO and the buoy, also serving as end stops within the PTO. Throughout these projects, 6-DOF industrial robots were employed as the primary machinery, with specific tools developed, constructed and validated for each task.

2.3 Robotics in education

Part of the thesis focuses on developing a laboratory module for the online teaching of the automation and robotics engineering course, which is included in various bachelor's degree programs, such as mechanical and electrical engineering. The course features several experiments based on real-world engineering projects, where students work in groups with industrial 6-DOF robots to conduct laboratory experiments and develop new automation solutions.

The aim of the project was to create lab exercises that can be utilized in a simulation environment, which also enables their use in online courses.

2.4 Desalination of sea water

A smaller portion of this thesis contributes to a larger project focusing on the use of WEC systems or a hybrid approach combining both WECs and solar energy to power a desalination facility. Specifically, the investigation pertains to a desalination park in Kilifi, Kenya. Wave data from Kilifi during 2015 is analyzed to estimate the potential power output from renewable energy sources. The study was conducted in an indoor environment, utilizing a scale model of the desalination device, which was powered by either a Direct Current (DC) unit or a 12 V battery. Water premixed with sea salt was drawn from a tank and pushed through the desalination device.

The purpose of this study was to investigate the power consumption concerning water quality and the possibility of utilizing the WEC to supply a desalination plant.

3 Industrial 6-DOF robot as dry test rig

3.1 Introduction

The PTO system is a crucial component in converting wave energy into electricity. A comprehensive evaluation is necessary to ensure the reliability and efficiency of various PTO designs before deploying them at sea. Traditionally, researchers have conducted tests in open-sea environments, which can be costly, time-consuming, and heavily reliant on wave and wind conditions [53-55]. To address these challenges, scaled prototype testing in wave tanks has been employed [56-58]. While wave tanks provide a controlled environment, they have inherent disadvantages, including the need for significant space, high operational costs, and challenges in accurately replicating sea wave formations with precise periods and amplitudes.

3.1.1 Dry test rigs

Currently, various types of dry test rigs are also used to evaluate wave power technology, differing in design and construction. A dry test rig is an equipment developed to assess and analyze a particular component, mechanism, or system under dry regulated conditions. It enables engineers and researchers to replicate operating conditions and evaluate performance, durability, and functionality before ocean and wave tank implementation or deployment. Most of these dry test rigs operate passively and do not consider hydrodynamic force effects as WECs do in reality [59- 64]. While this can be advantageous in the early development stages, a thorough analysis of the concept requires an active influence of hydrodynamic forces to effectively prepare for wave tank and open sea tests. Presently, only a limited number of dry test rig concepts have integrated hydrodynamic models into their evaluations [56, 64]. Existing dry test rigs are often limited in flexibility. They are generally customized systems that allow only a single DOF at the time, making them less flexible to replicate complex wave dynamics. Additionally, these rigs typically have stroke lengths ranging from 0.3 to 1.5 m and can handle outputs of up to 35 kW, limiting their ability to accurately simulate the full range of forces and wave climates encountered in real marine environments.

A variety of dry test rigs are currently employed for the evaluation of WECs, each offering specific advantages and limitations. The primary types of dry test rigs are hydraulic and electric.

Hydraulic test rigs are commonly used for testing WECs [65, 66]. The advantage of hydraulic rigs lies in their capacity to handle high-force applications. However, they also have some disadvantages, including higher operational and maintenance costs, as well as complex control systems needed to maintain accurate wave profiles.

In contrast, electric test rigs utilize electric motors to produce motion and replicate wave patterns [56, 60]. These rigs are simpler than their hydraulic counterparts. They provide exceptional motion accuracy, quick responsiveness to movement, and ease of control. Nevertheless, electric test rigs may face limitations in managing large forces compared to hydraulic rigs.

Despite their benefits, dry test rigs have notable limitations. They frequently face difficulties in large scale testing for WEC concepts, and the efficient integration of hydrodynamics into the system could be complicated. When hydrodynamics is integrated, the results may not fully accurately reflect the actual conditions found in open-sea and wave tank environments. As a result, many researchers and engineers prefer wave tank testing as a reliable method for evaluating various WEC designs in earlier stages during development.

A need for enhancing the flexibility and usability of dry test rigs has been identified. This includes to be able to use customized wave motions and different WECs in several DOFs. Also to be able to assess WEC concepts easily in early stages with more efficiency regarding time and costs in an industrial and scalable setup.

3.2 Robot test rig concept and experimental setup

The dry test rig investigated and developed in this project utilizes an existing 6-DOF industrial robot as testing equipment. The purpose of this test rig is to assess and analyze various WEC point absorber designs. This testing enables the evaluation of the WEC concept in several DOFs and facilitate the adjustment for various test conditions.

This project utilizes an ABB 6-joint industrial robot model IRB6650S, which has a payload capacity of 200 kg and a vertical reach that extends from 3 m above to 1.7 m below the robot's base, achieving a repeat accuracy of 0.14 mm. The robot test rig, developed for laboratory applications (see Figure 3), enables effective testing and evaluation of various point-absorber WEC concepts.

The robots outermost joint, joint 6, is controlled to emulate the movement of a buoy on the sea's surface in real-time. A hydrodynamic model is implemented within the robot control system to calculate the real-time hydrodynamic force imposed on the buoy. The calculation depends on the predefined parameters for the buoy and PTO, along with the tension force measurement in the wire linking the PTO to the robot's sixth joint.

By connecting the WEC-PTO systems to the robot's sixth joint the robot can replicate the motion of a buoy, thereby simulating the operational dynamics of WEC. This versatile test rig design supports a range of wave motions and buoy dimensions, which can be easily adjusted through software, allowing for various predefined wave motion patterns, buoy types, and sizes.

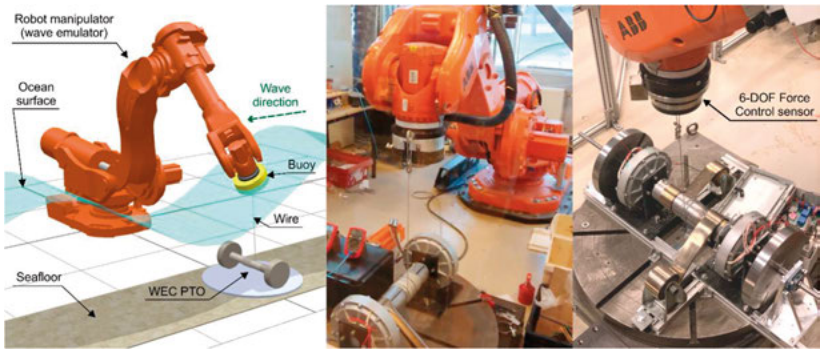

Figure 3: Robot test rig setup for LRTC-WEC testing in laboratory setting [Paper III]

3.2.1 Scaling

The robot's limitations regarding stroke length and payload necessity the scaling of WEC concepts. The dimensions of the PTO to be tested are determined by the limitations of the test rig, including its payload capacity and stroke length. A critical factor in scaling PTO is friction, which is difficult to scale accurately and significantly influences the result. In WEC applications, inertial and gravitational forces typically prevail, resulting in a scaling method based on Froude's scaling law [67-68]. By this concept, the Froude number (F_{nr}), as delineated in Equation 1, has to be constant between full-scale and scaled models. To achieve a more realistic result, the aim is to maximize the scale.

$$F_{nr} = \frac{U}{\sqrt{gl}} \tag{1}$$

where U is the relative speed of the WEC body with respect to the wave motion, g is the acceleration of gravity, and l is the characteristic dimension of the WEC.

In test rigs, a scaled WEC of 1:10-100 is frequently employed; however, a 1:4 scale is recommended for more accurate results [57]. The scaling size is unique to each concept, as the dimensions of the concepts can vary. Presently, industrial robots are available for purchase that can manage loads of up to 2300kg, including the ABB and Fanuc brands, having payload capacities of 1000kg and 2300kg, respectively, with stroke lengths of 3.5m and 3.7m. More details can be found in Paper III.

3.3 Use of the robot test rig

To our knowledge, no one has previously employed an industrial robot in a similar application (see Figure 4). The robot test rig has been utilized in two different modes: passive and active modes.

In passive mode, the robot can function as a test rig by encoding a motion sequence into its control system, enabling it to execute the program independently of its connection to the PTO or the buoy's force impact.

The test rig was used and evaluated in this configuration to effectively assess the functionality and performance of the LRTC-WEC concept, as described in Section 3.4.

In active mode, the robot's movement is influenced by hydrodynamic forces that vary according to the buoy's properties and the PTO specifications.

Utilizing the robot test rig in active mode is difficult due to multiple influencing aspects and the necessity for real-time force computations, more detailed descripted in Section 3.5.

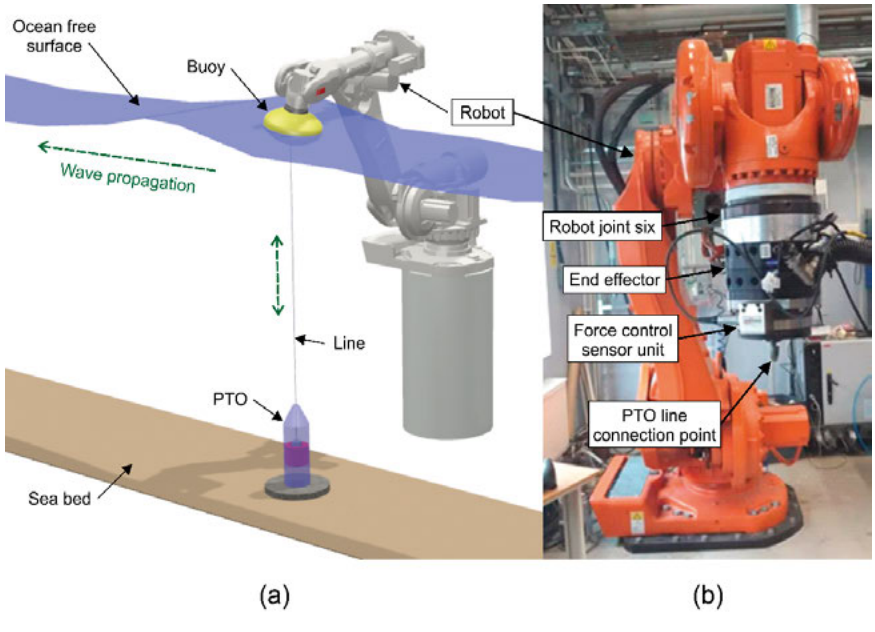

Figure 4: The robot test rig for UU-WEC evaluation: (a) conceptual illustration on the left, and (b) setup in the laboratory on the right [Paper VI].

3.4 The robot test rig in passive mode

The testing process was conducted in several phases, beginning with the robot's vertical movement in the heave direction. This assessment focused on both the mechanical design and energy output of the LRTC concept. Passive testing was conducted by repeating recorded buoy movements with multiple DOFs.

The initial phase of the practical investigation involved the formulation of the LRTC-WEC concept (see Figure 5) to serve as a PTO for the development of the robot test rig.

As the robot moves upward, it pulls on generator 1, while the spring enable the rotation of generator 2 as the robot descends. Through this repetitive motion, the robot alternates between upward and downward movements, causing both generators to rotate in opposing directions.

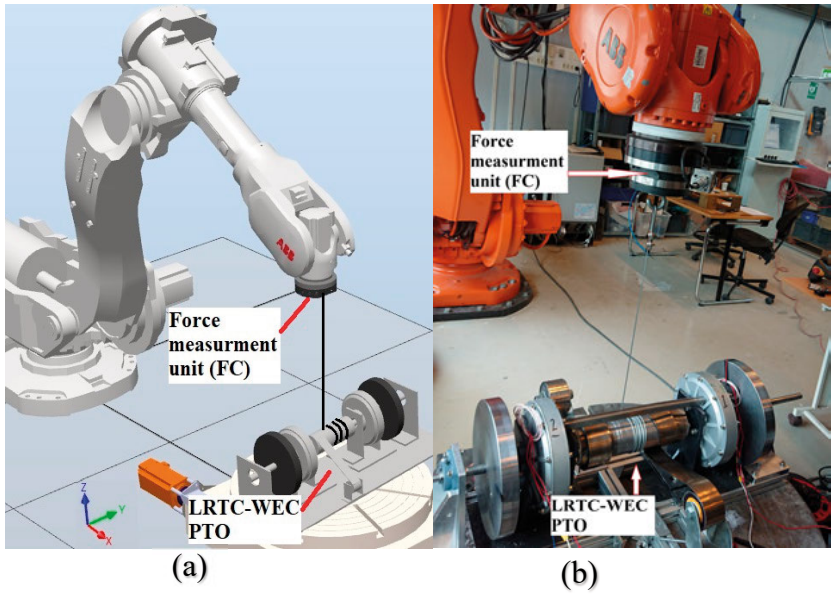

Figure 5: The robot test rig with an integrated force measurement unit. (a) On the left, the robot test rig setup in the simulation software RobotStudio, and (b) on the right, the robot test rig setup in the laboratory [Paper IV].

To conduct a thorough investigation of the test rig, it was essential to load the LRTC-WEC and measure the power output. This enabled comparison between the robot's movement and the power output generated by the LRTC-WEC. Since the generators operate on three-phase Alternating Current (AC), the power output was rectified and connected to passive loads, specifically power resistors of 33 ohms for each generator, which is the maximum load

specified for the generators. A measurement board was developed to specifically measure current, voltage, and the traction force in the wire. The data collected was processed using the PC LabVIEW software. Figure 6 provides an overview of the setup parts.

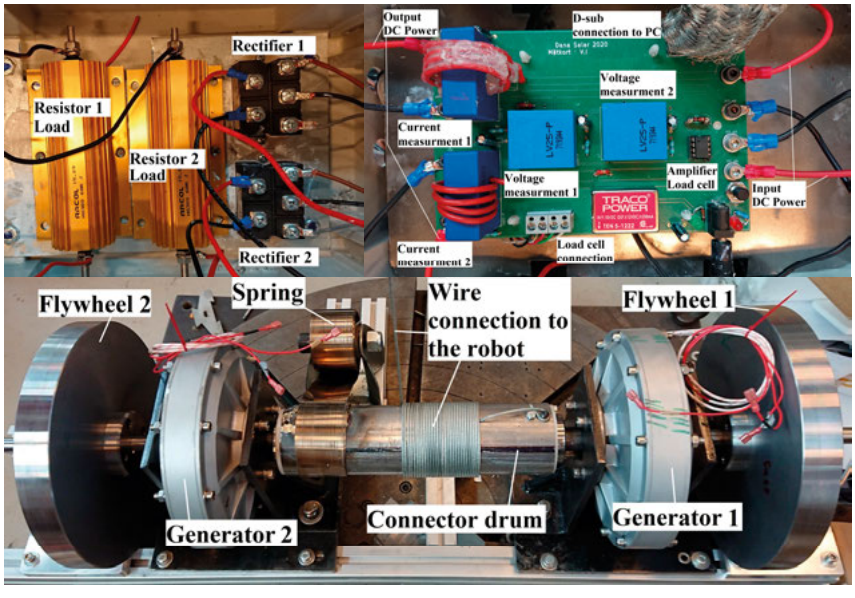

Figure 6: Overview of the LRTC-WEC setup and measurement board. The top left section displays both the rectifier and passive loads for the generators. The top right section features the measurement card, while the bottom part displays the LRTC test concept as implemented in the laboratory [modified from Paper II].

To enhance the LRTC design, flywheels were incorporated to ensure more smooth power output and to store excess energy. Initially, the robot test rig operated in a passive manner, during these phases. A standard sine wave with varying amplitude and period was employed, along with studies involving irregular wave motions, to further assess the LRTC concept.

3.5 The robot test rig in active mode

The robot test rig in active mode allows it to function as a real buoy on the sea surface. During this phase, testing has been conducted exclusively in the heave direction with a single DOF; however, the test rig is capable of accommodating up to 6-DOF. A hydrodynamic model is necessary for the test rig to dynamically adjust its position in response to hydrodynamic forces.

Three primary forces affect the buoy (see Figure 7): the hydrodynamic force exerted by the buoy (F_{hyd}), the acceleration force acting on the buoy (F_{buoy}), and the mechanical and damping forces from the WEC-PTO (F_{mec}).

By Newton's second law, the buoy's acceleration is calculated, with the buoy's mass represented as m_b and the acceleration $\ddot{z}(t)$.

$$F_{buoy} = m_b \ddot{z}(t) \tag{2}$$

$$m_b \ddot{z}(t) = F_{hyd} + F_{mec} \tag{3}$$

The hydrodynamic force F_{hyd} calculates active on the buoy based on its equilibrium location. It comprises three primary components: the hydrostatic force F_h, the excitation force F_e, and the radiation force F_r, which is calculated from the wave motion.

$$F_{hyd} = F_h + F_r + F_e \tag{4}$$

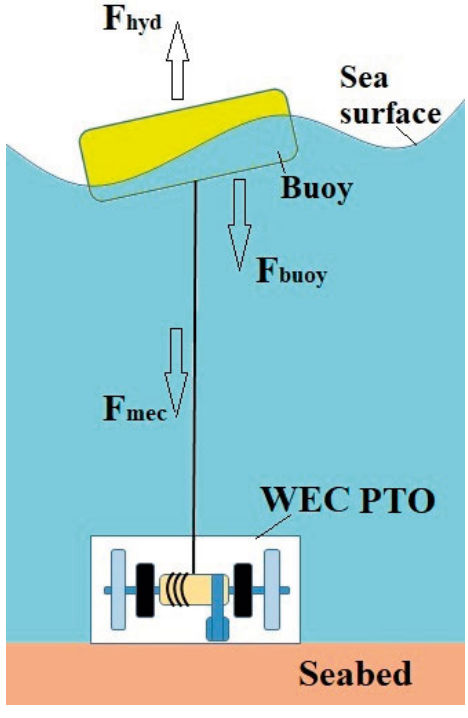

Figure 7: Hydrodynamic force impact on the buoy on the sea surface.

Subsequently, two different active control methods were developed and evaluated: the force control method and the position control method. Subsections 3.5.1 and 3.5.2 elaborate on the successful execution of these theoretically defined procedures.

3.5.1 Force control method

The force control method requires the robot controller to compute a reference force based on the current position of the robot. The robot aims to achieve this computed force during its movement. It begins from a defined position, determined by a predefined wave height input into the control system. The actual position of the robot is continuously monitored by the robot controller, allowing the calculation of velocity through deriving the actual position of the robot. Further deriving of the velocity gives the acceleration, from which the acceleration force of the emulated buoy can be calculated with Newton's second law.

In real-time, the hydrodynamic forces are calculated by integrating a hydrodynamic numerical model within the robot controller (see Figure 8). The model reference force $F_{ref2}(t)$ is then computed by summing all the calculated hydrodynamic and WEC forces.

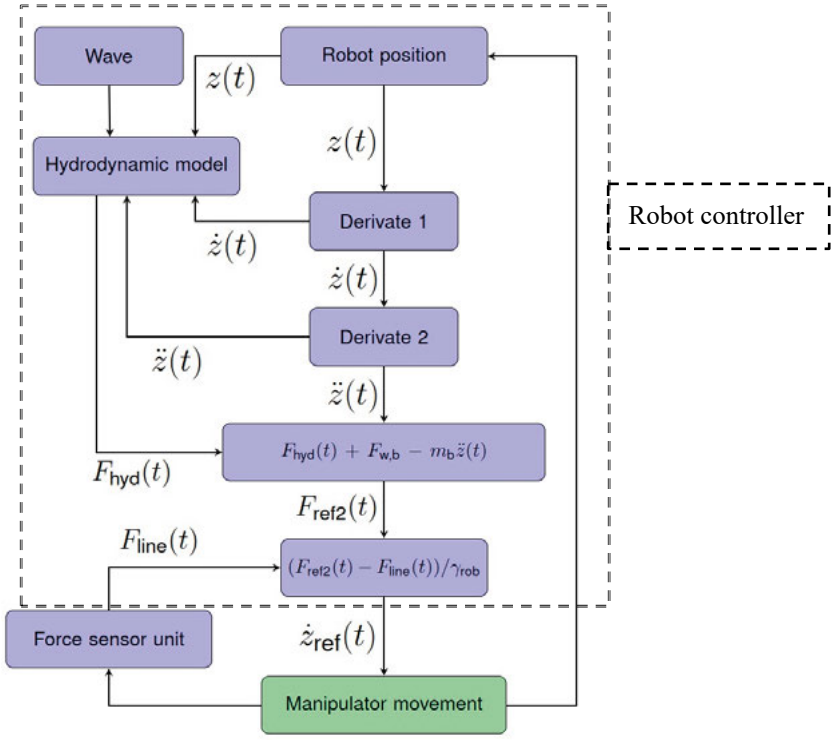

Figure 8: Schematic of implemented hydrodynamic force control model in the robot control system [modified from Paper VI].

3.5.2 Position control method

The robot control system gathers all data, including the force measurement in the wire, to calculate the robot's position (see Figure 9). The robot control system receives a defined wave motion in real time. The calculation of the hydrodynamic force acting on the buoy is based on an estimated initial buoy position and wave motion. At the same time, the force sensor unit reads the pulling force of the wire between the robot and the PTO. Newton's second law is used to calculate the acceleration of the buoy given the net force acting on it. This value is integrated to update the speed of the buoy and integrated again to calculate the position. The robot implements the position as a manipulator movement. Ultimately, the robot uses the updated motion results to recalculate the hydrodynamic force and continuously generates a new wire tension force. This approach allows the robot controller to emulate the position of the buoy in real time.

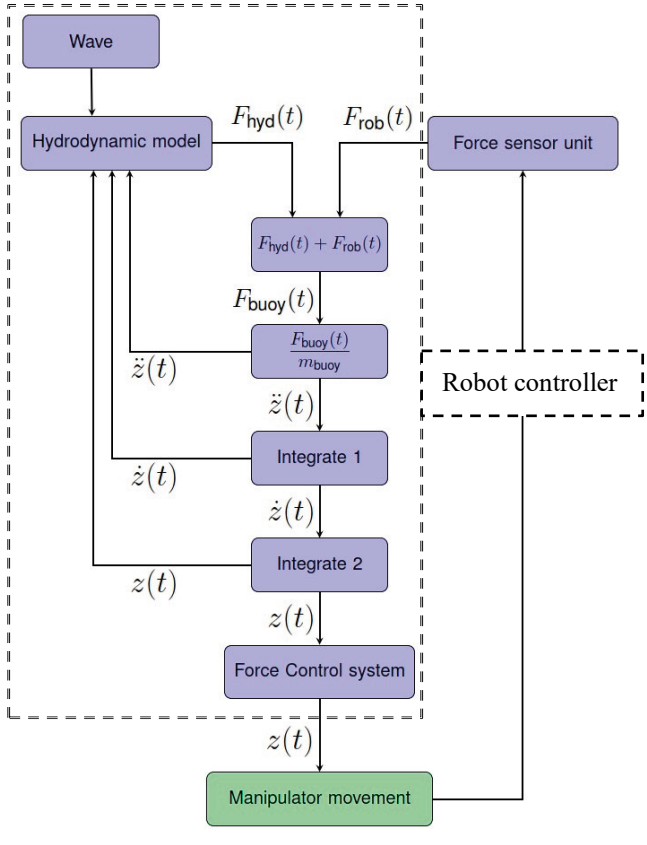

Figure 9: Schematic of implemented hydrodynamic position control model in the robot control system.

3.5.3 Hydrodynamic model

A hydrodynamic model has been seamlessly integrated into the controller system of the robot. This model enables the robot to emulate the motion of a buoy on the sea surface, responding dynamically to various stresses produced by ocean waves.

The hydrodynamic forces experienced by the buoy depend on its configuration, dimensions, and the mechanical and damping forces exerted by the PTO system, along with the characteristics of incoming sea waves [69-71].

The hydrodynamic model implementation has been continuously developed and improved. Parameter calculations differ depending on the character of the wave motion model, whether regular or irregular.

Note that we used different terminologies for position, velocity, and acceleration across the numerous publications. Some sources identify them as x, $\dot{x}$ and $\ddot{x}$, while in others identify them as z, $\dot{z}$ and $\ddot{z}$. This thesis consolidates the designations into z, $\dot{z}$ and $\ddot{z}$.

In the following calculations, it is important to note that the parameters F_e and IRF are derived from the known shape of the wave motion. Conversely, F_h and F_r are computed in real time.

3.5.3.1 Hydrodynamic calculations used for regular wave motion

The model is based on a buoy positioned on the sea surface moves in the heave direction, in only one DOF. The model includes calculation for the forces influencing buoy movement (see Figure 7), calculates the buoy's acceleration force utilizing Equation 3, measures the tension force in the wire which equals the total mechanical PTO forces, and derives the hydrodynamic force using Equation 4 [69]. This model is a simpler hydrodynamic framework, simplifying implementation without consideration of time history; however, the time history is less relevant to regular wave motions. This model was only used for tests using LRTC-WEC as a PTO. The following calculation is a condensed version from Paper III.

We calculate the forces F_h, F_r, and F_e from Equation 4 using the following Equations 5-8.

$$F_h = \rho g A_s z(t) \tag{5}$$

$$F_r = A_m(\omega)\ddot{z}(t) + B_c(\omega)\dot{z}(t) \tag{6}$$

Where ρ is the liquid density, g is the acceleration of gravity, A_s describes the transverse area of the buoy, *z(t)* is the vertical displacement of the buoy, A_m is the added mass, B_c is the damping coefficient, ω is the wave angular frequency, $\dot{z}(t)$ is the buoy velocity and $\ddot{z}(t)$ is the buoy acceleration.

The excitation force for regular wave as uses in this project is:

$$F_e = \Gamma(\omega)\frac{H_s}{2} sin\omega t \tag{7}$$

Where Γ(ω) is the force amplitude and H_s is the significant wave height:

$$\Gamma(\omega) = \sqrt{\frac{2g^3\rho B_c(\omega)}{\omega^3}} \tag{8}$$

The Boundary Element Method (BEM) solver Wave Analysis developed at the Massachusetts Institute of Technology (WAMIT) provides the added mass and radiation damping [72-73].

3.5.3.2 Hydrodynamic calculations used for irregular wave motion

The hydrodynamic model used for the irregular waves is based on the point absorber WEC from Uppsala University [74], as depicted in Figure 10. This study focuses the modelling of the UU-WEC in 1-DOF in heave motion. The computational derivation presented here is a summary taken from Paper VI.

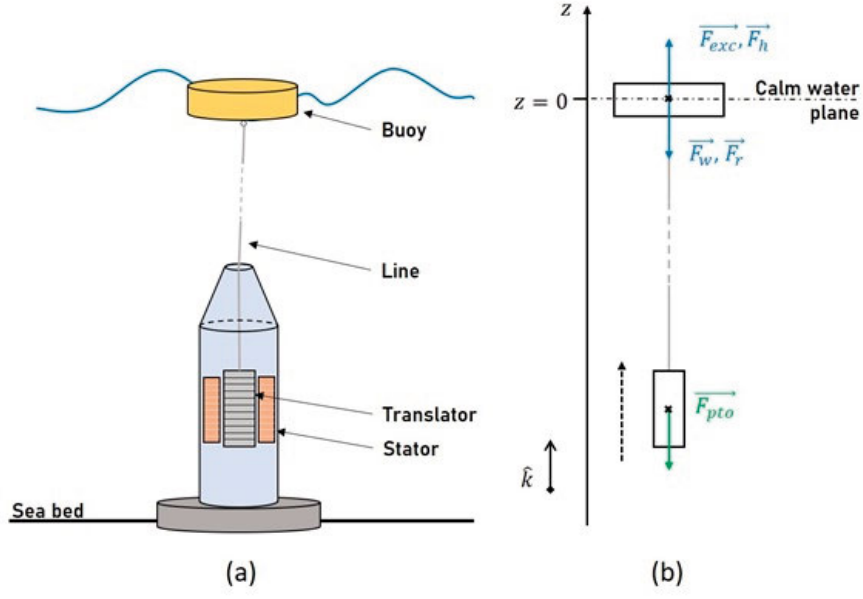

Figure 10: (a) Schematic of the Uppsala University wave energy converter, and (b) Representation of modeled forces as vectors [Paper VI].

The following equation is similar to Equation 3; however, the parameters represents differently.

$$m_{wec}\ddot{\boldsymbol{z}}(t) = \boldsymbol{F}_{hyd}(t) + \boldsymbol{F}_{w} + \boldsymbol{F}_{pto}(t) \tag{9}$$

where $\ddot{\boldsymbol{z}}$ represents the WEC's acceleration, $\mathbf{F}_{\text{hyd}}$ represents the overall hydrodynamic force exerted on the buoy. The $\mathbf{F}_{w}$ and $\mathbf{F}_{pto}$ signify the WEC's weight and the PTO force. The mass of the WEC is equivalent to the sum mass of the buoy and PTO, defined as $m_{wec} = m_b + m_{pto}$.

The following equation is the same as Equation 4. However, it is presented again due to differing nomenclature.

$$\boldsymbol{F}_{hyd}(t) = \boldsymbol{F}_{exc}(t) + \boldsymbol{F}_{r}(t) + \boldsymbol{F}_{h}(t) \tag{10}$$

The excitation force in time domain is defined as the convolution product between the excitation impulse response function (IRF) $f_{exc}(t)$ and the wave surface elevation $\eta(t)$ at the buoy location,

$$\boldsymbol{F}_{exc}(t) = \hat{\boldsymbol{k}} \int_{-\infty}^{\infty} f_{exc}(t-\tau)\eta\,(\tau) \tag{11}$$

where $\hat{\boldsymbol{k}}$ is the unit vector positive in the upward direction. The excitation IRF is found from the inverse Fourier transform of the excitation force coefficients $f_{\omega,e}(\omega)$,

$$f_{exc}(t) = \frac{1}{2\pi}\int_{-\infty}^{\infty} f_{\omega,e}(\omega)e^{i\omega t}d\omega \tag{12}$$

The radiation force is given by the convolution product between the modified radiation IRF $f'_{rad}(t)$ and the buoy velocity $\dot{\boldsymbol{z}}(t)$ plus the corrective added mass term at infinite frequency.

$$\boldsymbol{F}_{r}(t) = -m_{\infty}\ddot{\boldsymbol{z}}(t) - \int_{0}^{t} f'_{rad}(t-\tau)\dot{\boldsymbol{z}}\,(\tau)d\tau \tag{13}$$

where m_{∞} is the buoy's added mass at infinite frequency. The modified radiation IRF is expressed as

$$f'_{rad}(t) = \frac{2}{\pi}\int_{0}^{\infty} B(\omega)cos\,(\omega t)d\omega \tag{14}$$

where $B(\omega)$ is the buoy's radiation damping.

3.6 Validation of the robot test rig concept

The evaluation of the test rig concept involved several stages. Initially, the rig was assessed using a simulated model within the RobotStudio software (see Figure 11) and a numerical model created in Simulink MATLAB. Both control methods—force control and position control were thoroughly validated through a series of experiments with regular waves. These experiments included various wave motions and buoy sizes while utilizing the LRTC-WEC as the PTO system. More detailed information can be found in Papers II-V.

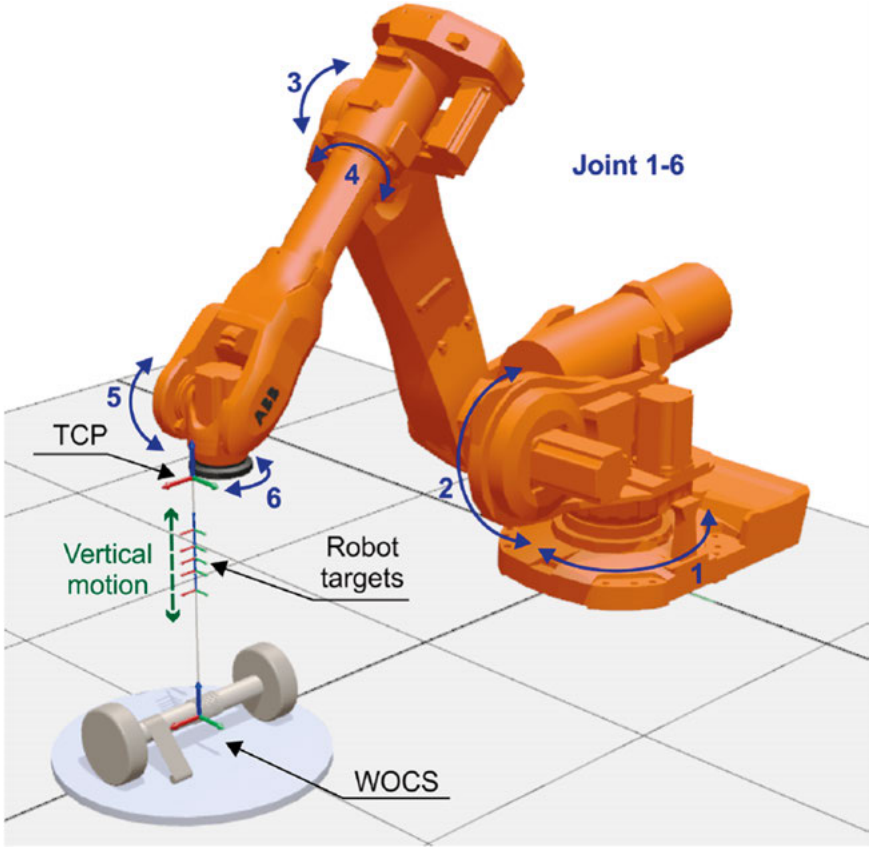

Figure 11: The robot setup in simulation software RobotStudio [Paper III]

Further analysis was performed to evaluate the test rig concept in the 1-DOF heave direction with irregular waves. This involved using a numerical model based on Linear Potential Flow (LPF) theory, implemented with the BEM solver WAMIT. The numerical model was evaluated against a wave tank experiment conducted at the Ocean Basin of Plymouth University's Coast Laboratory (see Figure 12) [75]. In this experiment, the PTO system employed was a linear eddy-current brake, which utilized an aluminum translator moving vertically within a constant electromagnetic field generated by magnets. Additional details regarding the wave tank experiments can be found in [76].

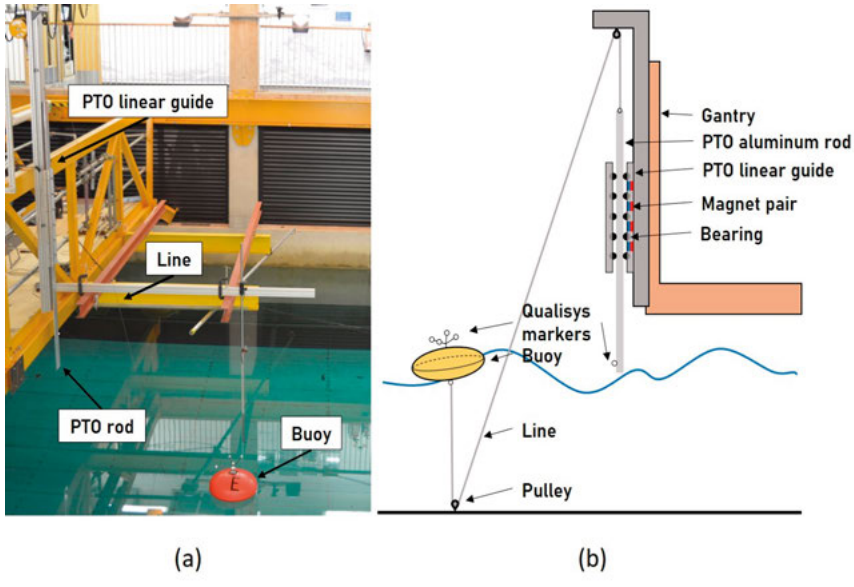

Figure 12: The UU-WEC schematic, with (a) wave tank setup (b) equivalent wave tank experiment is drawn [Paper VI].

The PTO force is modelled in the numerical model as a linear damper

$$\boldsymbol{F}_{pto}(t) = -\gamma_{pto}\dot{\boldsymbol{z}}(t) \tag{15}$$

where γ_{pto} is the PTO damping coefficient.

3.6.1 Implementation in the robot control system

This part of the study implements the hydrodynamic model for the force control method focusing on irregular wave motions using two different strategies: one for one-body model and another for a two-body model. The difference between one and two-body models in the context of force control methods is $\boldsymbol{F}_{ref}$. The robot test rig is designed to operate as a one or two-body system.

The calculation described below is a condensed version from Paper VI.

3.6.1.1 Two-body model concept implementation

The following calculation use $\boldsymbol{F}_{ref2}$ for two-body models.

$$\boldsymbol{F}_{ref2}(t) = \boldsymbol{F}_{hyd}(t) + \boldsymbol{F}_{w,b} - m_b\ddot{\boldsymbol{z}}_{\boldsymbol{b}}(t) \tag{16}$$

where $\boldsymbol{F}_{w,b}$ is the buoy weight, m_b is the buoy mass and $\ddot{\boldsymbol{z}}_{\boldsymbol{b}}(t)$ is the buoy acceleration.

$$\boldsymbol{F}_{line}(t) = \boldsymbol{F}_{pto}(t) + \boldsymbol{F}_{w,pto} + m_{pto}\ddot{\boldsymbol{z}}_{\boldsymbol{pto}}(t) \tag{17}$$

where $\boldsymbol{F}_{line}(t)$ represents the measured force. The robot's integrated force sensor unit directly measures the sum of the PTO damping force $\boldsymbol{F}_{pto}(t)$, the PTO weight $\boldsymbol{F}_{w,pto}$, and the PTO acceleration force $m_{pto}\ddot{\boldsymbol{z}}_{\boldsymbol{pto}}(t)$.

The robot control system subsequently regulates the calculated reference force $\boldsymbol{F}_{ref2}(t)$ as a target value. The Force Control system computes the disparity between the requested reference force $\boldsymbol{F}_{ref2}(t)$ and the actual measured force $\boldsymbol{F}_{line}(t)$, subsequently utilizing this information to determine a velocity reference $\dot{\boldsymbol{z}}_{\boldsymbol{ref}}(t)$ for the robot's execution.

$$\dot{\boldsymbol{z}}_{\boldsymbol{ref}}(t) = \boldsymbol{F}_{ref2}(t) - \boldsymbol{F}_{line}(t)\ ) \,/\, \gamma_{rob} \tag{18}$$

where γ_{rob} represents the robot damping coefficient set within the Force Control system. The robot therefore adjusts to meet the most recent reference force, necessitating a minimal damping coefficient to enhance responsiveness and reduce the damping effect on the performed motion.

3.6.1.2 One-body model concept implementation

Due to time and financial constraints, we were unable to reproduce an identical PTO system used in both the wave tank tests. Consequently, the theoretical damping coefficient was simulated using the robot's force sensor software, with results comparable to those of an ideal PTO damping.

Since a PTO was not implemented and there is no force feedback system, the system is considered to be a one-body model (see the schematic implementation differences in Figure 13).

The parameter calculations and hydrodynamic implementation strategy differ from the two-body concept, The PTO damping force $\boldsymbol{F}_{pto}(t)$ is now simulated by using the PTO damping coefficient γ_{pto} as the robot damping coefficient γ_{rob}. If assuming that $\dot{\boldsymbol{z}}_{ref}(t)$ is equal to $\dot{\boldsymbol{z}}(t)$ Equation 18 can rewrite, and $\boldsymbol{F}_{pto}(t)$ solves, then compares to Equation 15, resulting in

$$\boldsymbol{F}_{ref1}(t) = \gamma_{pto}\dot{\boldsymbol{z}}(t) \tag{19}$$

$$\boldsymbol{F}_{ref1}(t) = -\boldsymbol{F}_{pto}(t) \tag{20}$$

where $\boldsymbol{F}_{ref1}(t)$ is the reference force for the one-body model. This require that Equation 16 is rewritten to handle the PTO and buoy as a stiff body

$$\boldsymbol{F}_{ref1}(t) = \boldsymbol{F}_{hyd}(t) + \boldsymbol{F}_{w} - m_{wec}\ddot{\boldsymbol{z}}(t) \tag{21}$$

In this configuration, $\boldsymbol{F}_{ref1}(t)$ acts as the PTO damping force implemented in the robot controller. Although this approach does not include the effects of a physical PTO system, it simplifies the process of configuring and optimizing the PTO damping coefficient directly within the robot controller.

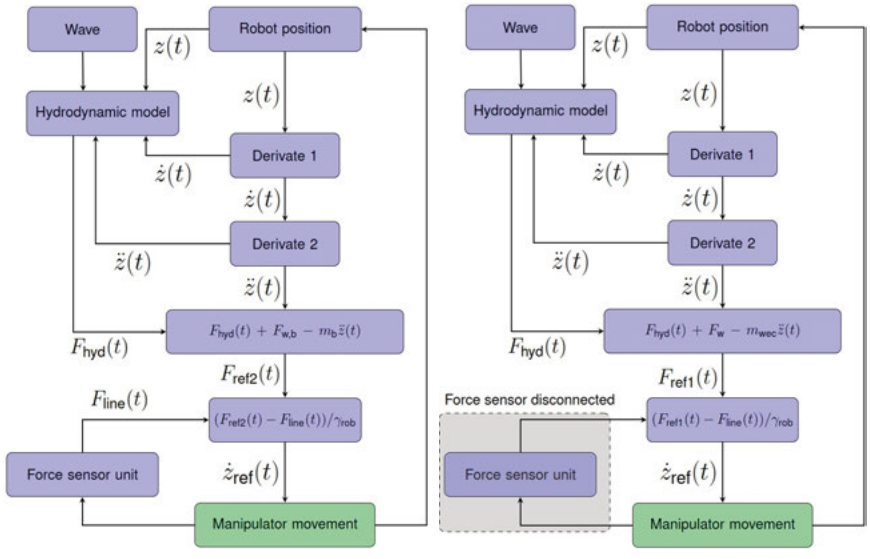

Figure 13: The control scheme of the robot with the hydrodynamic model implemented in force control model, with (a) is for two-body model, and (b) for one-body model [Paper VI].

3.7 Robot test rig fidelity

The robot system's repeatability of 0.14 mm allows for a manageable level of experimental variance, which is critical for accurate testing. To further assess the reliability of our results, an additional investigation was conducted, focusing on the magnitude of experimental error. This assessment took place during the final stage of our testing process.

During the stage, two distinct forms of wave motion examined specifically W_1 and W_2 and evaluated two variants of buoys B_1 and B_2. This comprehensive approach resulted in a total of four Study Cases (SC) (see Table 1), providing a framework for evaluating the test rig's performance under varying conditions. The selection of these SCs was determined by the constraints of the existing robot test setup, namely regarding stroke length, damping coefficient, and computational capability.

Table 1: Overview of Study Cases in final verification stage. This table summarizes the experimental conditions including wave height (H_s), wave period (T_p), buoy characteristics (name, shape, radius, height, and mass) for each study case conducted [Paper VI]

Study case	*Wave name*	H_s [m]	T_p [s]	Buoy name	Buoy shape	Radius [m]	Height [m]	Mass [kg]
SC_1	W_1	0.14	2.38	B_1	Ellipsoid	0.242	0.140	4.582
SC_2	W_2	0.25	3.52	B_1	Ellipsoid	0.242	0.140	4.582
SC_3	W_1	0.14	2.38	B_2	Cylinder	0.3	0.16	8
SC_4	W_2	0.25	3.52	B_2	Cylinder	0.3	0.16	8

The robot experimental outcomes were compared with the numerical model results for validation purposes. To estimate the accuracy of the test rig in relation to the numerical data, using the Normalized Root Mean Square Error (NRMSE), defined as:

$$NRMSE = \sqrt{\frac{\sum_k (y(k) - \hat{y}(k))^2}{\sum_k y(k)^2}} \tag{22}$$

where y is the true and $\hat{y}$ is the predicted value.

3.8 Results

The robot test rig developed through several stages, ensuring validation and functional verification at each stage.

Initially, the robot was employed as a test rig to verify the LRTC-WEC concept, as detailed in Papers I and II. In this stage, the robot was validated as dry test rig operating in a 1-DOF heave direction, utilizing both regular sine waves and recorded irregular wave patterns, without feedback from force measurements in the wire connecting the PTO to the robot. At this stage, the robot will follow the path of the wave motion. Figure 14 displays results from an experiment focused on the LRTC-PTO power output.

In the second stage, the robot test rig was enhanced by integrating an advanced force sensor that measures wire tension and provides this data back to the robot's control system. This enhancement enabled the development and implementation of a hydrodynamic model within the test rig, allowing the robot to emulate buoyant behaviour on the sea surface actively, resulting in more realistic outcome. Figure 15 illustrates the active robot motion in 6-DOF, which is part of the results from Paper III.

Two distinct hydrodynamic models were implemented: one for positional control and another for force control methods, and validated, as outlined in Paper III.

Stage three focused on demonstrating and assessing the active interaction in the dry test rig, for the force control method, and the LRTC-WEC functioning as a PTO in a 1-DOF scenario. Figure 16 presents the results of the experiment from Simulink and the robot test rig for two distinct cylindrical buoy sizes (see Table 2), which also illustrates the control delay in the force F_r for the robot test rig against the corresponding simulation in Simulink, as outlined in Paper IV. The control delay primarily results from the inability to adequately modify the damping sensitivity.

In stage four, our focus shifted to the position control method, crucial for avoiding control delay and increasing the damping sensitivity without destabilizing the system.

An issue with the position control method was addressed, characterized by a control lag that caused system imbalance when the robot encountered larger forces or significant wave motions.

Figure 17 illustrates the robot's control lag incidence relative to the buoy's dimensions and wave motion. Figure 18 shows the simulation results from Simulink, illustrating the impact of control lag on system instability.

A new method of control has been developed utilizing EGM [77], enabling reduced control lag. The procedure has been validated through simulation in RobotStudio, as described in Paper V.

In the final stage, the implementation of a new hydrodynamic model for active buoy emulation with irregular wave motion was assessed. The model has been validated against wave tank testing (see Figure 19), more details can be found in Paper VI. The force control method was used in 1-DOF heave motion, as detailed in Paper VI.

Table 2: Buoy parameters used in experiments in stage three [Paper II]

	D (m)	h (m)	m (kg)	A_m (kg)	B_c (Ns/m)
Buoy 1	1.2	0.5	100	550	180
Buoy 2	0.6	0.5	25	64	12

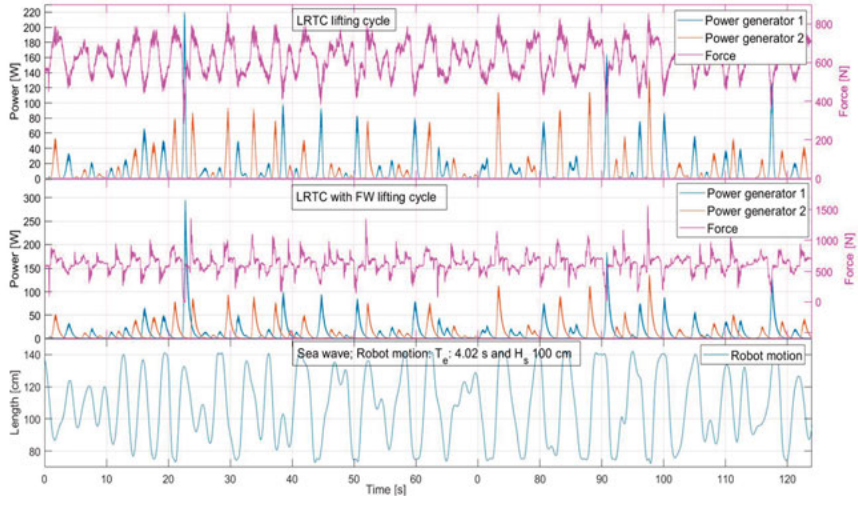

Figure 14: The LRTC lifting cycle series. Sea wave motion with *Hs* = 1.0 m and T_e = 4.02 s [Paper II]

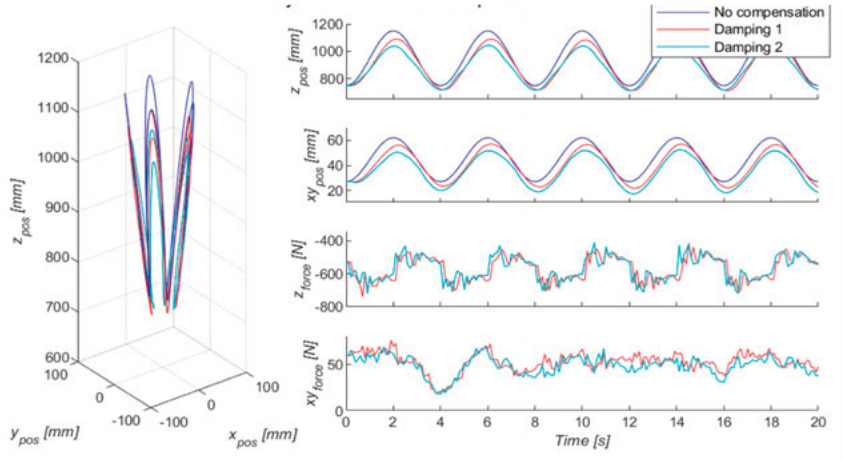

Figure 15: Illustrate the robot motion in 6-DOF with real-time force response with regular sinusoidal motion with vertical amplitude 200 mm and period time 4 s in position control [Paper III].

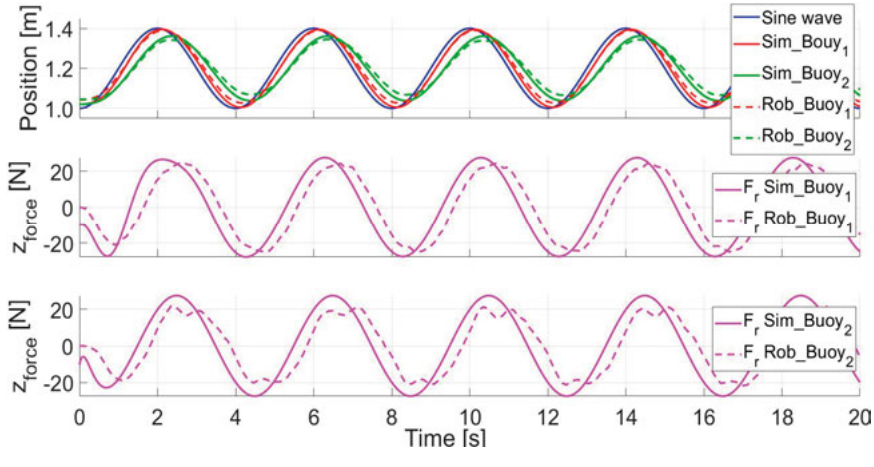

Figure 16: Experimental result illustration of a lag in the robot test rig experiment relative to the simulation experiment in Simulink [modified from Paper IV].

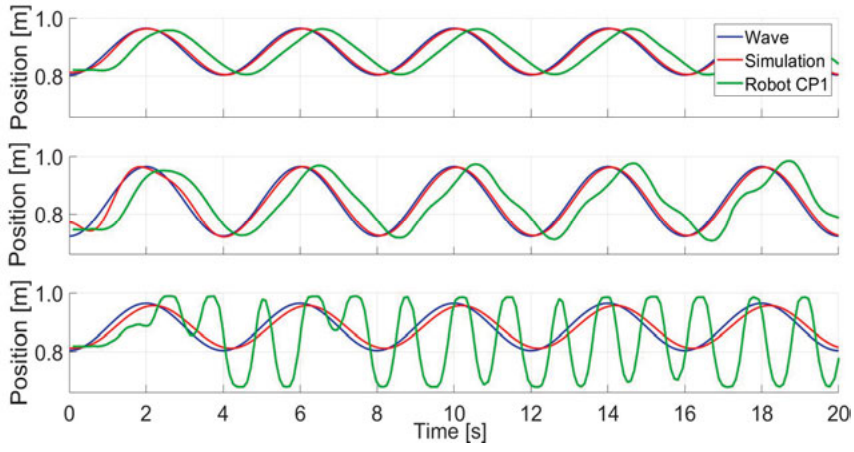

Figure 17: Simulation and robot experiments based on wire force measurements (CP1) motion results for wave 1 and buoy 1 (top), wave 2 and buoy 1 (middle) and wave 1 and buoy 2 (bottom) [Paper V].

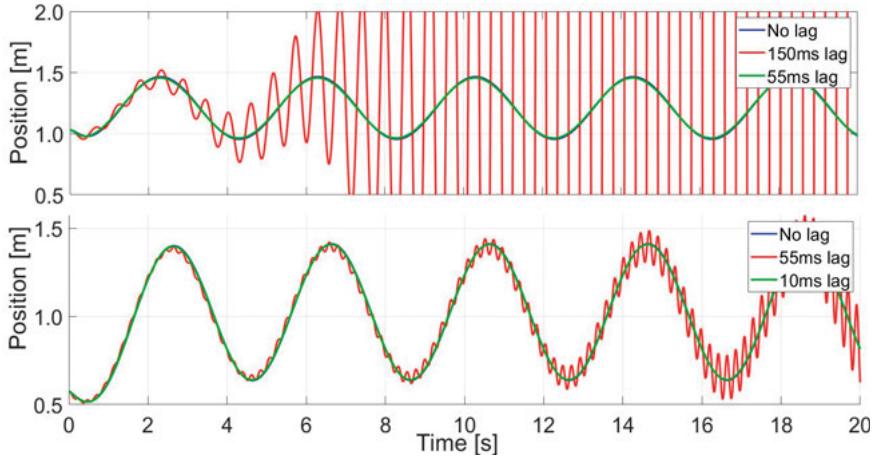

Figure 18: Simulation motion results for different simulated control lags for wave 2 and buoy 2 and theoretical wire force 800 N/(m/s) (top) and for wave 2 and buoy 2 with increased theoretical wire force to 2500 N/(m/s) (bottom) [Modified from Paper V].

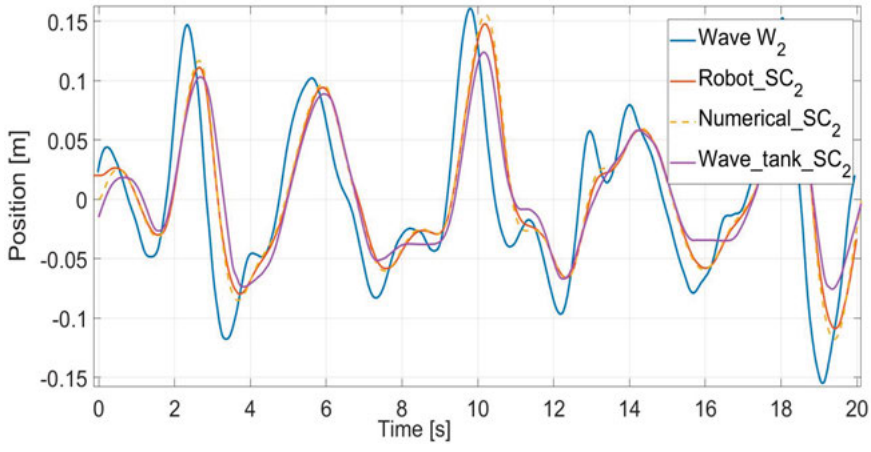

Figure 19: Comparative analysis of results from the robot, wave tank, and numerical model simulation studies for SC_2 [Paper VI]

To assess the test rig's motion fidelity in relation to the robot's repeat accuracy of 0.14 mm, a mean NRMSE was calculated based on 50 runs per case compared to the numerical simulation result in the final stage validation. The results are illustrated in Figures 20 and 21, with a detailed overview provided in Table 3. The stability of the model can also be emphasized over several iterations, the result of which is that the deviation is very small; Table 3 provides a detailed overview. For the computation of NRMSE, 18 s from the total 20 seconds were used, adjustments made for the 1.5 seconds needed for the robot to stabilize and the exclusion of the final 0.5 seconds for the same stabilization process. Also, a piecewise cubic spline interpolation was utilized to eliminate time step inconsistencies, aligning the sample rate with the numerical model results.

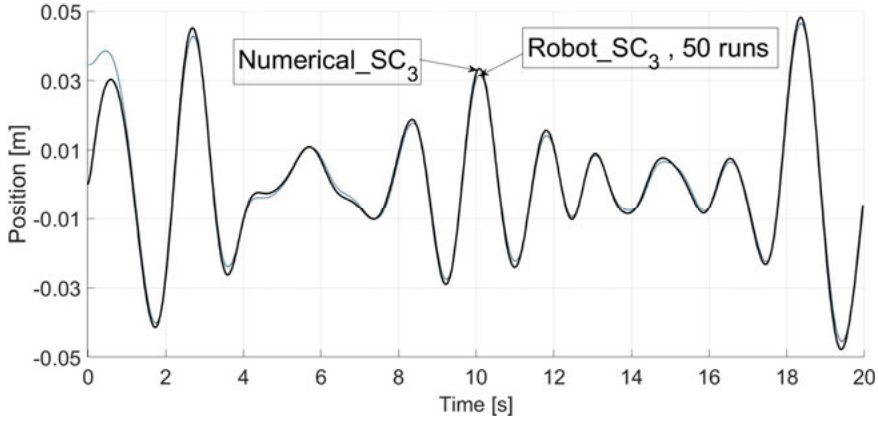

Figure 20: Numerical model SC_3 in comparison with Robot SC_3 (50 runs) [Paper VI]

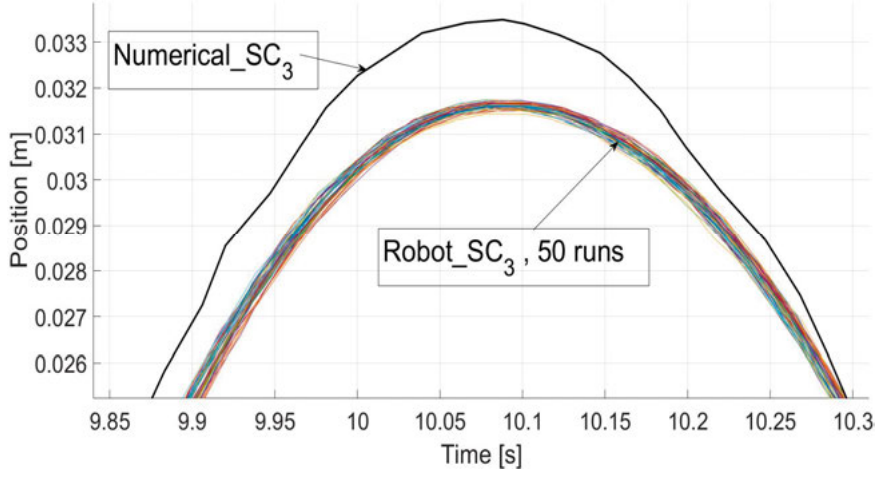

Figure 21: Zoomed part of Figure 19, Numerical model SC_3 in comparison with Robot SC_3 (50 runs) [Paper VI]

Table 3: NRMSE for robot SC of 50 runs for each study case, numerical SC as predicted value and robot SC as true value [Paper VI]

True value Numerical model	Mean NRMSE robot vs Numerical model [%]	Standard deviation robot 50 runs [%]
SC_1	8.4	0.0316
SC_2	5.8	0.0349
SC_3	8.6	0.0454
SC_4	5.9	0.0208

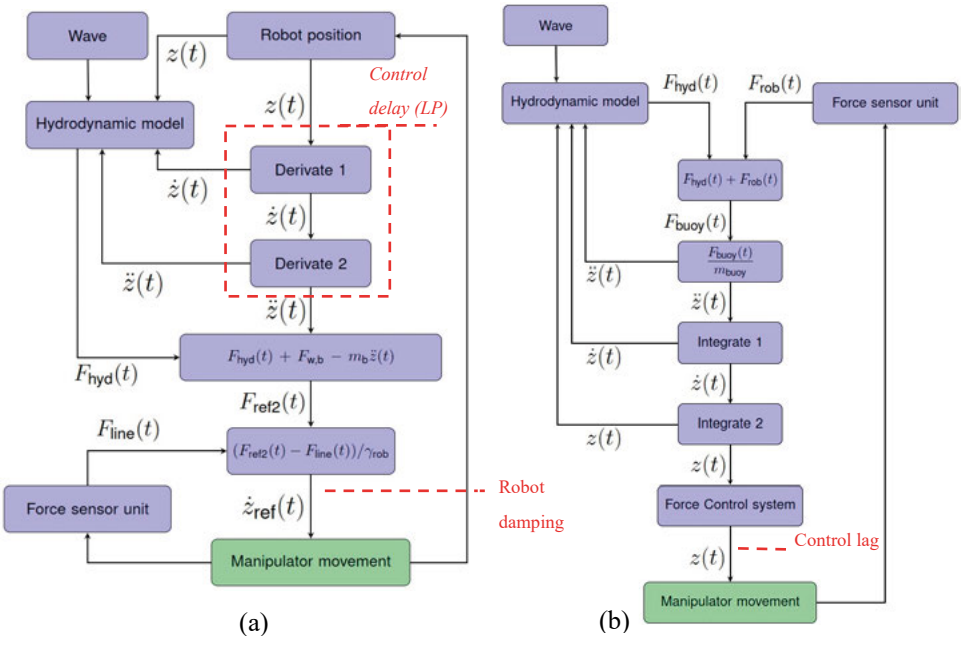

Figure 22: A schematic illustration for the hydrodynamic implementation in the robotic test rig system. With (a) where it is marked in red where lag in the LP filter arises in the force control method and (b) where it is marked in red where control lag arises for the position control method [Modified from Paper VI].

3.9 Discussion

The test rig's development went through multiple phases to achieve an effective, stable solution.

Stage one focused on evaluating the LRTC-WEC concept, using the test rig as passive testing equipment. At this stage, the primary challenge was to assembly and adapt the LRTC and measurement components to ensure the concept operated effectively. The challenge was to integrate both hardware and software, especially when it comes to achieving consistent interaction throughout the system.

Stage two successfully implemented a hydrodynamic model into the test rig by utilizing a 6-DOF force sensor of ATI brand, which was compatible with our robot control system. This stage involved assessing the system's constraints and validating the entire test rig design, including both control strategies: force control and position control, under minor wave oscillations.

Several challenges were discovered with both methods used. A control delay associated with the damping setting was seen in the force control method, while a control lag of 500 ms was noted in the position control method.

Stage three investigations conducted investigations to determine the magnitude of the motion accuracy error associated with the force control system. Figure 16 illustrates the results of the study, highlighting difficulties related to the force control method in current robot systems. The robot's motion induces a control delay condition due to the inability of the damping sensitivity setting to be sufficiently maximized. In our instance, connecting a real PTO to the robot ideally aims to set damping to 0; nevertheless, this results instability of the test rig system.

The delay may also be influenced to a lesser extent by the radiation force F_r. The robot's position influences speed and acceleration, which are subsequently LP filtered to achieve stable values. As a result, the velocity and acceleration are derived with a certain delay, subsequently influencing the computed value of F_r. Enhanced deviations were observed with larger PTO forces or faster movements.

Stage four investigated the position control method's limitations concerning control lag (see schematic discerption at Figure 9) and suggested a suitable solution. The result from Figure 17 indicate that reducing response time decreases the motion stability issues related to control lag but may slightly increase motion accuracy error and overshoot. The upper motion plot illustrates the robot's motion response to the calmest wave and the largest buoy. The outcome aligns closely with the simulation, except for the control lag. However, the medium wave and large buoy in the central plot show slight movement instability. In the lower figure, characterized by the calmest wave and

the small buoy, it is clear that the robot begins to overshoot, leading to instability. The design of the control system limits the robot's movement within 700 to 1400 mm for safety purposes.

The outcomes of the simulation experiments illustrated in Figure 17 confirm that control lag can induce instability. While minimizing control lag reduces instability risk, it necessitates a compromise in movement precision. The robot showed a control lag of 500 ms, impacting its movement and potentially causing system instability. The lower diagram of Figure 18 exemplifies that a fivefold increase in wire tension force is needed to induce instability at a control lag of 55 ms for the investigated setup.

Figure 18 illustrates the results of analyses conducted using the simulation software Simulink, demonstrating that a solution developed via EGM systems that minimizes control lag to 10-20 ms could be sufficient to stabilize motion response. The EGM method was confirmed through RobotStudio simulation software but could not be executed on a physical robot system due to the system's lack of support for the EGM option.

In the last stage, the implementation of the hydrodynamic model was upgraded for irregular wave motion. The results from the test rig were validated with a numerical model specifically designed to evaluate the UU-WEC concept through four study cases. In the absence of an EGM system and the inability to use the position control method, we used the force control method, which theoretically aligns with the position control method. The numerical model validated the test rig at this stage. The results (see Figure 19) indicate that the robot's movement aligns more closely with the numerical model than the numerical models align with the wave tank experiment. To enhance the robot test rig, it is essential to optimize the numerical model.

The hydrodynamic model implementation was updated by incorporating additional buoy shapes, an ellipsoidal buoy. Since in this investigation it is important how long-time history (decay time) is used in the calculations, an investigation was made due to the previously mentioned robot's computational capacity related to the radiation force calculation, Figure 23 displays the result.

So far, the computational capacity of the test rig has not been a crucial concern in the investigations, since the issue was successfully addressed through calculation optimization and convergence analysis. In the future, when experiments are performed with several DOFs in real-time hydrodynamic response, this factor significantly influences the outcomes.

This test rig concept has significant potential for the assessment and evaluation of several WEC concepts, especially considering intentions to enhance it with a larger robotic system and support for real-time control response. While the test rig cannot exactly emulate wave tank or open ocean trials, it can serve as an essential preliminary equipment for such studies. The test rig can be utilized, particularly at the initial stage of WEC development, where the mechanical components and conceptual design are assessed. Furthermore,

the test rig can potentially be utilized for the optimization of the concept's mechanical efficiency and power output.

The repeatability and accuracy of the robot test rig were also assessed. The low standard deviation indicates that the robot test rig performance is stable (see Table 3). Each of the four study cases was tested 50 times to assess variations across different trials. The study case $SC_{1,3}$ had a higher mean NRMSE than study case $SC_{2,4}$, possibly due in part to the greater impact of an equal position deviation relative to some larger wave motion in $SC_{2,4}$.

Figures 20 and 21 display the results of the study, highlighting significant discrepancies at the peaks of the graph.

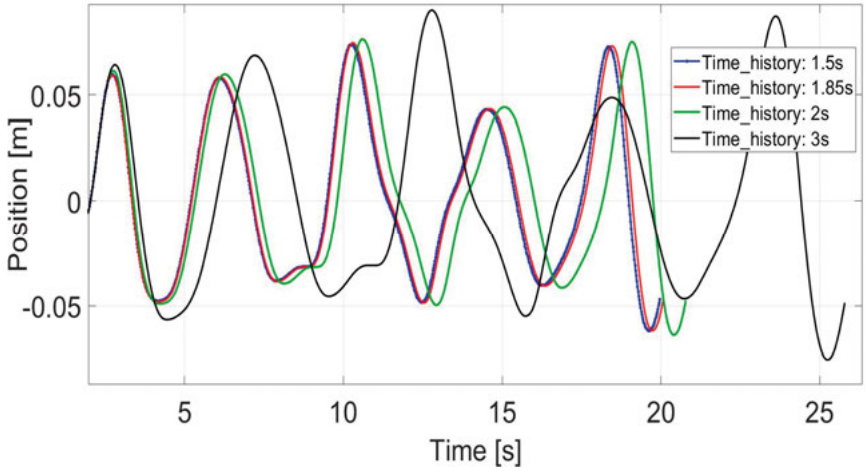

Figure 23: Tests with different history times (decay time) were made, where the movement with a 1.5s history time is used as a reference to the remaining movement [Paper VI].

3.9.1 Limits and potential solutions

During the development process, several limitations have been identified. While some have been resolved or appropriate solutions found, others persist. The primary limitation of the test rig is the robot's payload capacity, which is restricted to 200 kg. The average payload is satisfactory for our experimental setup; nevertheless, because to the imperfections of the LRTC-PTO, spiky forces and snap loads arise during assessment, significantly impacting the size of the force. In the early stages of assessing the LRTC-WEC at maximum load, we utilized smooth and slow wave motions to prevent exceeding the designated payload during acceleration. This issue can be mitigated by avoiding maximum loading of the PTO or using a smaller scale.

Another issue identified in stage four relates to the force control method showed that the robot damping sensitivity setting parameter hindered accurate motion emulation. The primary objective in our case was to minimize robot damping, hence increasing response sensitivity; however, this maximization of response sensitivity resulted in overall system instability (see schematic implementation description Figure 22.a).

The position control method faces a similar challenge. The robot controller calculates the next target for the robot and transmits it to the manipulator. However, a control lag about 0.5 s can result in an unbalanced test rig. A proposed approach for position control method is to implement real-time control via the EGM system.

Heavy computations challenge the robot's computational capabilities. The issue occurs when calculating the radiation force F_r for irregular wave motion, which relies on the duration of the time history. Figure 23 demonstrates that the maximum history time the robot can manage without overloading for F_r is 1.5 s. To address this, a proposed solution is to perform the computation of F_r externally, utilizing an EGM system data receiver that operates with a sample interval of 4 ms, which is expected to resolve the issue.

4 Robotized production technology of the UU-WEC generator

4.1 Background

All products, including WECs, require efficient planning for large-scale manufacturing to facilitate the production of many units within a realistic timescale. Uppsala University created the UU-WEC technology and subsequently evaluated its production in Lysekil on the West Coast. During the development phase, the UU-WEC experienced significant changes in components and specifications, resulting in the fabrication of several UU-WEC versions. The manufacturing of the UU-WEC was painful and inefficient, considering the intended deployment of these units throughout multiple parks, each with a capacity of up to 1000 units. To create an effective production line that meets company requirements, the automation of production was required. A research project was started on automated manufacturing of the UU-WEC alongside its manual production. The entire production process was examined, and the possibility of automating the most relevant sections was investigated. More details can be found in Paper VII.

4.2 Robotized production of UU-WEC

The initiatives to automate UU-WEC production (see Figure 24.a) initially overlooked the most monotonous, tiring, and risky components of the concept. The stator coil and the translator represent the two primary components of the UU-WEC. Rubber discs are an auxiliary component of the PTO. These discs are employed at the end stops to reduce the translator's stop forces, while other discs are combined and integrated into the connection wire to avoid snap loads in the wire (see Figure 24.b). The stator coil production includes two main assemblies: stator stacking and stator winding, both of which started the automation research project [78-79]. The focus in this thesis is translator magnetization and rubber disc cutting.

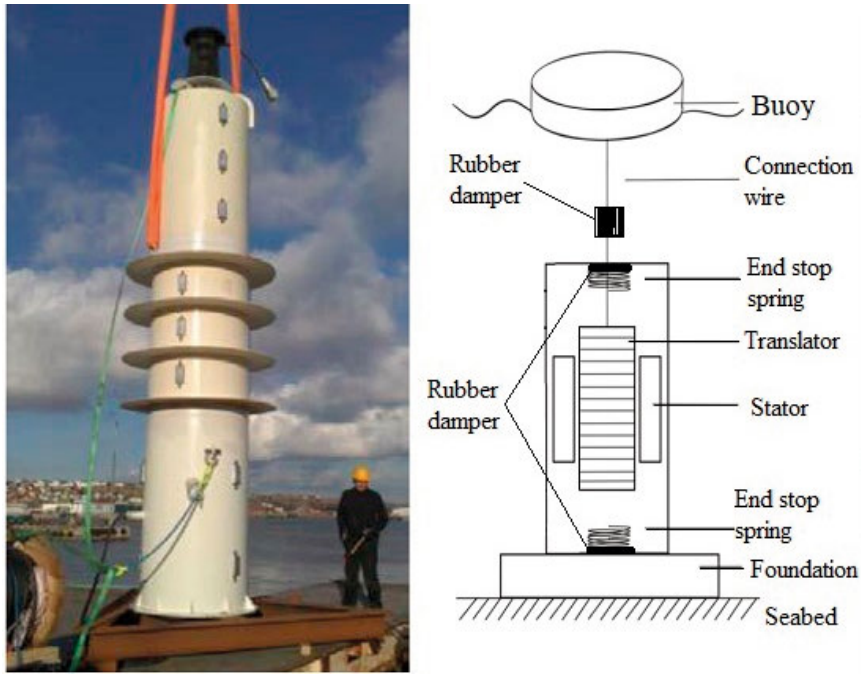

(a) (b)

Figure 24: The UU-WEC, (a) in the left shows the complete PTO, and (b) in the right describes UU-WEC inside components [modified from 80]

4.2.1 Magnetizing of the translator

Permanent Magnets (PMs) are often used instead of rotor windings in electric rotating machinery. PM machines provide a simplified design, reduced maintenance, and increased power density; but, they forfeit the ability to adjust rotor magnetization [81-82]. Alternative techniques for affixing PMs to rotors include gluing or clamping [83-84]. The construction of larger PM rotors is often done manually; however, automated methods are available [85-87].

The translator in UU-WEC corresponds to the rotor in a rotating generator; it is 3 meters in length and has 8 side plates, each size 3000 x 200 mm, on which the magnets are surface mounted (see Figure 25.A). A total of 848 $Nd_2Fe_{14}B$ PMs is included in each translator, each PM sized 115 x 47 x 11 mm. The assembly was conducted manually using a plastic wedge and rubber hammer, whereby the magnet was positioned, and the rubber a hammer was used to secure the final few millimeters if required (see Figure 25.B and C).

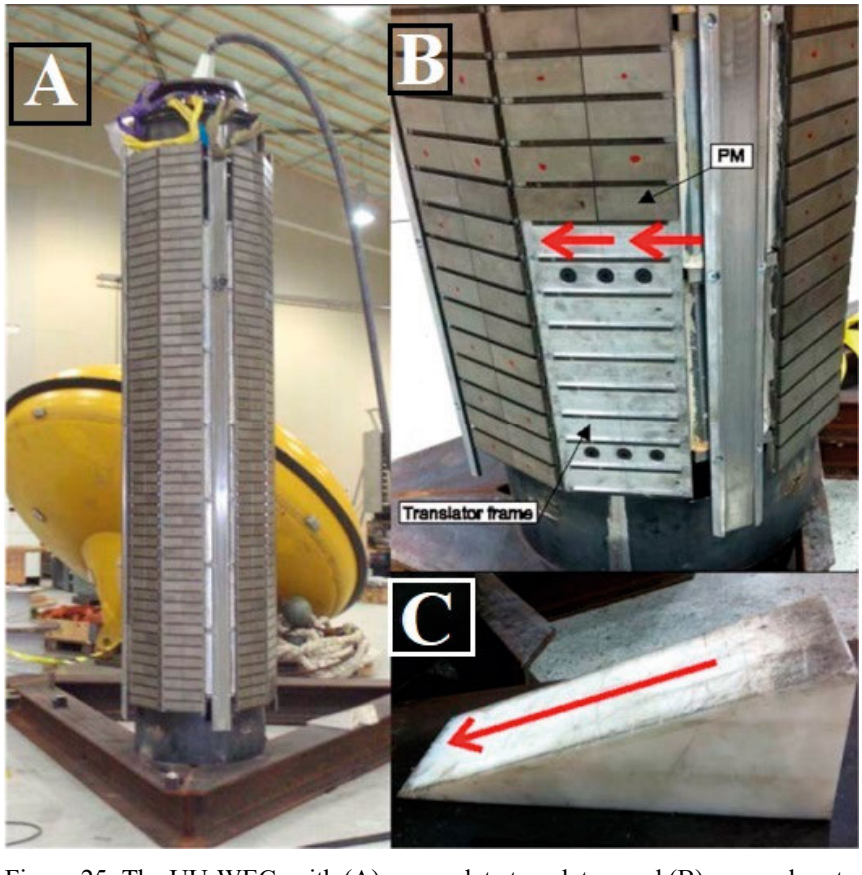

Figure 25: The UU-WEC, with (A) a complete translator, and (B) zoomed part of translator, and (C) is a wedge tool for manual magnetization [Paper VIII]

The manual magnetization process was difficult, tiring, and time-consuming due to the large number of magnets and the magnet's strong pulling force. A PM in a 2 mm air gap constitutes the equivalent of 75 kg of pulling force against the translator housing.

A complete production robot cell solution was developed and simulated using RobotStudio (see Figure 26).

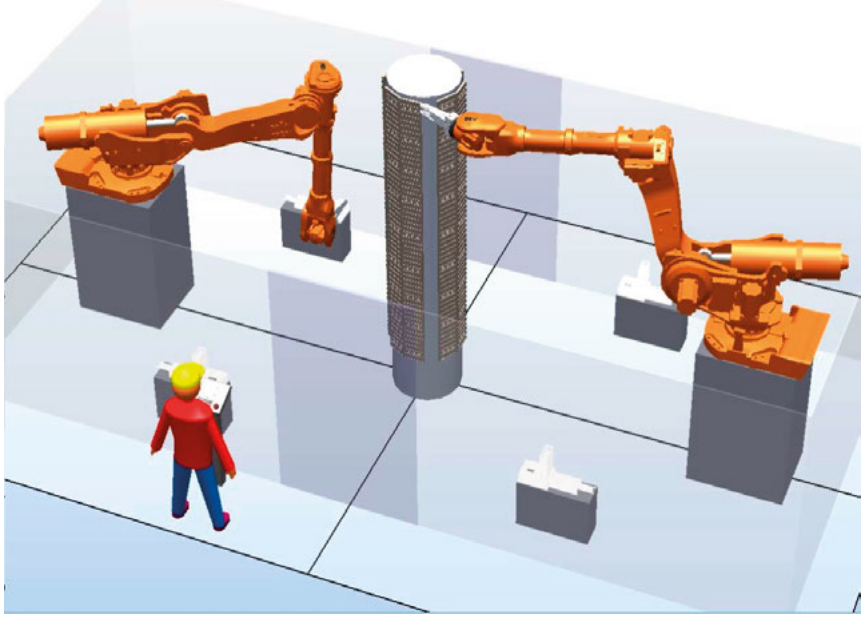

Figure 26: Automated solution in the software RobotStudio [Paper VIII]

A robot tool solution was developed and constructed for implementation on a 6 joint industrial ABB robot 6-DOF of the model IRB6650s. The method was based on a manual work process in which the magnet is pushed from a non-magnetic wedge into position on the translator's side surface. The tool is made of aluminium and includes small steel rollers along the edges, designed to secure the magnet by magnetic field forces. A motorized push mechanism positions the magnet downward with constant velocity (see Figure 27).

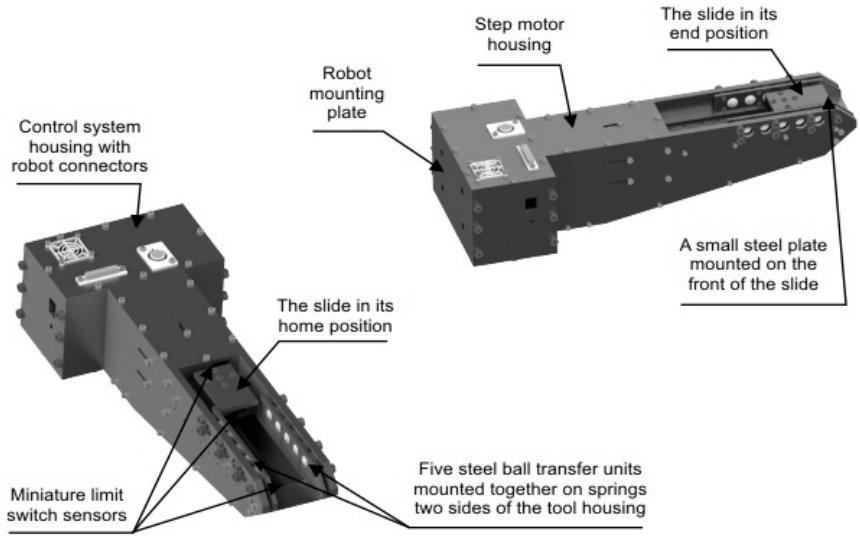

Figure 27: Tool for automated magnetization purposes [Paper VIII]

A solution proposal for the magnet supply within the robot cell was developed and constructed (see Figure 28). The magnet magazine test concept is designed to contain 10 PMs, with wooden spacers separated to avoid direct contact between them. A pneumatic piston functions as the mechanism within the magazine, delivering a PM during its outward motion and collecting the wooden spacer during its inward motion.

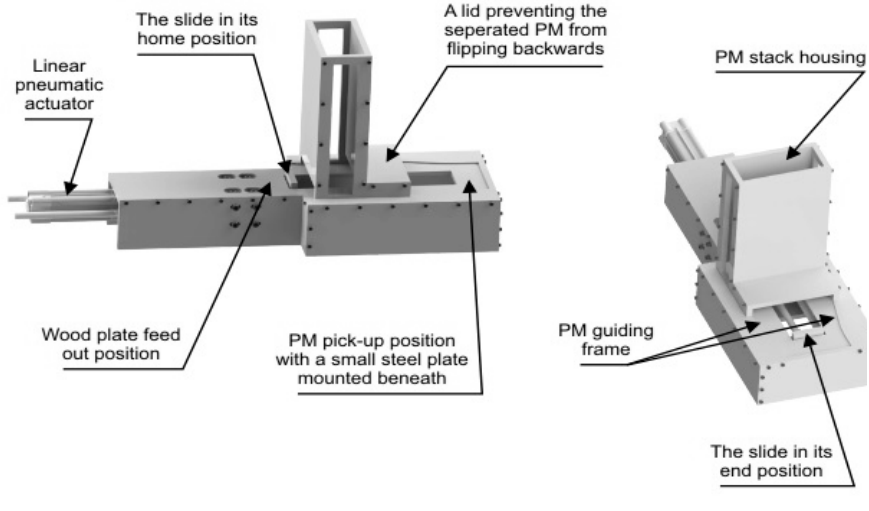

Figure 28: Magnet magazine tool, developed for deliver store about 10 PMs and delver one by one to the robot [Paper VIII]

Subsequently, both the robot tool and the magnet delivery tool were validated in a laboratory environment using an existing 6-DOF industrial robot, ABB model IRB4400, with a payload capacity of 60 kg and a reach of 1.96 m (see Figure 29), more detailed can be seen in Paper VIII.

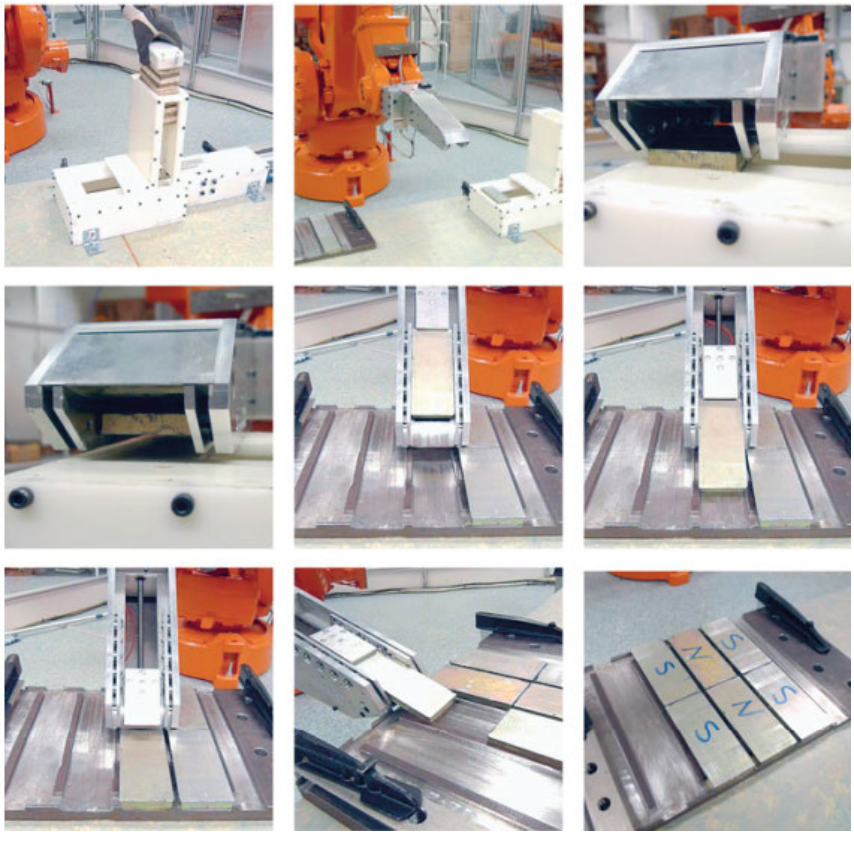

Figure 29: An overall view of the tools during the PM assembly process [Paper VIII]

4.2.2 Manufacturing of rubber component

A UU-WEC contains a total of 64 rubber parts made of Ethylene Propylene Diene Monomer (EPDM). The rubber discs have an outer diameter of roughly 250 mm, an inner diameter of approximately 100 mm, and a thickness of 25 mm. Two people were manually involved in the manufacture of the UU-WEC rubber discs. A smaller rubber sheet is cut from a bigger rubber roll, following which the discs are stamped with a manual hydraulic press and a metal cutting punch. This task is tiring and time-consuming, thus requiring automation. Considering the low dimensional accuracy requirement, the discs can be processed by an industrial robot instead. In contrast to conventional Computer Numerical Control (CNC) machinery, robot processing offers more flexibility but lower accuracy, along with more complex programming requirements. Research indicates the necessity for mechanical upgrades and advancements in robot motion control and programming tools, including specialist Computer-Aided Manufacturing (CAM) software, to solve issues associated with high accuracy robotic machining in hard materials [88-92].

A simpler method could be developed for cutting UU-WEC rubber discs by utilizing a milling machine tool connected to an ABB 6-DOF industrial robot, model IRB6000. The milling tool was attached to the robot's outermost joint, besides a simple tool designed for collecting cut rubber discs (see Figure 30). For further details, see Paper IX.

Figure 30: Rubber disc milling solution [Paper IX]

5 Robotics in education

As a PhD student at Uppsala University, some of duties in the Division of Electricity included supervising a course automation and robot engineering. The course included several parts, including several lab exercises where students engaged with 6-DOF. Technological developments worldwide are progressing swiftly, requiring corresponding adaptations in education to meet modern demands. Modern engineering requires collaboration, practical inventiveness, ongoing education, adaptability, and a focus on sustainability [93-100]. Throughout the instructional period, I engaged in modifying and enhancing specific components of the course, including the practical laboratory aspects. With the emergence of the COVID-19 pandemic, it was immediately determined that all educational activities should transition to an online format. Most institutions faced significant challenges [101-103].

The course continued basically as previously, however adapted for an online distance learning format. The most challenging aspect was developing practical lab tasks in the simulation software that corresponded with those conducted on-site (see Figure 31). The labs could be finalized, and the students successfully fully examined online; however, the laboratories could not replicate the actual on-site experience. Paper X provides more details into this work.

Figure 31: Robot in the real lab environment and in the simulation environment for online teaching.

6 Use of WEC for desalination of sea water

More than 70% of the Earth's surface is covered in sea waters, and roughly 40% of the global population resides near coastal areas [104]. Although all sources of water are accessible, 4 billion people experience a scarcity of fresh water at parts of the year [105]. Currently, the conversion of seawater into drinking water is made easier by a desalination equipment. The procedure involves the circulation of saltwater through the desalination unit, which extracts salt from the water and delivers fresh water and which will require an energy source for operation. Desalination Parks (DP) are often powered by fossil fuel electricity. Researchers are increasingly investigating the use of Renewable Energy Sources (RES) for powering desalination parks [106-107]. Solar and wind energy are the majority of renewable energy in distributed power DPs [108-110]. The study of WECs combined with desalination as RES for DP operation is of interest due to their direct correlation [111]. This could be utilized off-grid and in remote coastal regions or islands. Small-scale systems could also be developed for disaster resilience, where there is a need to rapidly ensure access to clean water [112]. This work focuses on the specific wave data from 2015 at Kilifi, Kenya.

A scaled prototype of a desalination system was connected to perform experiments and evaluate the concept (see Figure 32). A 12 V DC power supply was used to supply the desalination unit in the experiment. The 12V power source functions as a scaled power reservoir for the WEC unit.

The experiment aimed to investigate the effects of pressure in relation to water quality, hence affecting energy usage for the Reverse Osmosis (RO) system.

A manual gauge was used during the experiments to adjust the system pressure from 0 to approximately 7 MPa. The measurements (using a TDS measurement unit that measures in PPM and degrees Celsius) included the salinity and temperature of the incoming water and the salinity of the generated fresh water. An analogy flow meter was used to measure the flow rate of the desalinated water. At a constant voltage of 12 V and an incoming water salinity of about 35 ppt at a temperature of 20°C, the results showed that freshwater production started at about 2 MPa. As the pressure escalated, the salinity of the generated water decreased significantly, falling below the 500 ppm standards for safe drinking water, although it eventually reached close to 6 MPa.

The current increased approximately linearly with pressure, varying from 70 A to 160 A at pressures up to 7 MPa. Freshwater flow rose above 3 l/min with increasing power but decreased at maximum power levels. More information about the results and performance can be found in Paper XI.

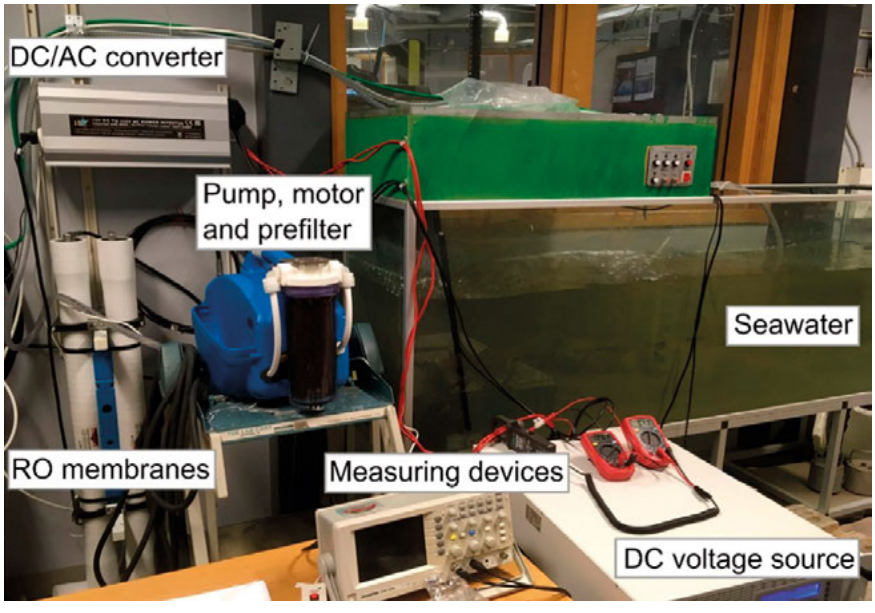

Figure 32: The setup for the experiment contains a tank with saltwater (35 ppt), measurement equipment, and a desalination system including RO [Paper XI].

7 Conclusion

This chapter presents the conclusions from the previous chapters. Each topic will be assigned its own section and linked to the study objectives.

7.1 Industrial 6-DOF robot as dry test rig

A robotized 6-DOF dry test rig concept with an integrated hydrodynamic model for testing and evaluating various types of point-absorber WEC concepts in 1-DOF (heave) has been developed and validated.

This test rig allows for the use of a variety of wave types, both regular and irregular, as well as the use of different buoy shapes. It can easily be used for repeated WEC performance tests. The concept has been systematically validated through multiple phases.

In Paper III, an extensive overview and validation of the dry test rig concept is provided. Both force control and position control methods were introduced, evaluated and validated.

In Paper IV, the interaction of the robot test rig with the LRTC-WEC as PTO was examined in detail for the force control method with regular waves. An obstacle was identified wherein the robot's integrated damping sensitivity could not be entirely maximized; increasing damping sensitivity results in a swifter response, although simultaneously risks causing the robot to become unbalanced.

In Paper V, a corresponding investigation was conducted for the position control method. The primary emphasis was on control lag, and a suggested approach was developed for minimizing it.

In Paper VI, the test rig was developed to also manage irregular wave motions, using the force control method and a simulated UU-WEC PTO. An upgrade of the hydrodynamic model was implemented in the robot control system, which was evaluated against a numerical model. The numerical model was in turn evaluated against wave tank experiments. The results showed that the robot test rig follow the numerical model better than the numerical model did against the wave tank experiment results.

7.2 Robotized production of UU-WEC

Solution proposals for the assembly of PMs and rubber discs production for the UU-WEC has been developed and key steps has been validated. A variety of tools and equipment have been developed to support fully automated robot solutions. More investigation is required before integrating the robot cells on a production line.

7.3 Robotized production in education

The work outlined a well-planned educational transition from campus-based to entirely online education. The challenge stemmed from the course's practical learning methodology. All stages for online implementation were successfully created, including video capturing, clear instructions, and new simulation software models.

7.4 Use of WEC for desalination of sea water

Wave data from Kilifi, Kenya in 2015, as well as experimental data from a RO system demonstrator, were given to discuss the viability of RES to supply RO systems. The experimental investigation provided clarity to analyze the possibilities that wave energy resources from Kilifi, Kenya could power a suitable RO system.

8 Future work

The main investigation in this thesis focuses on the dry test rig, this development continues and therefore suggested future work is given focused on the test rig.

I. First, we should make use of the robot's 6-DOF by developing and implement a hydrodynamic model for several DOFs, which improves fidelity compared to full-scale tests in the open sea. Such a model requires faster computing capacity, which requires an upgrade of the robot's control system. Alternatively, the hydrodynamic model can be moved from the robot's control system to an external device, which can quickly calculate the position of the buoy and feed it back to the robot.

II. Upgrade the robot test rig by integrating an EGM system for the position control method to enable real-time control.

III. A larger robot with an increased payload capacity, would facilitate the testing of WECs in a larger scale.

IV. Another interesting option is that the test rig system continues to be developed for another application:

- A Monitoring Control System (MCS) is intended to monitor a buoy on the open sea or in a wave tank that is connected to a mechanically controlled damping in real time.
- The robot test rig system receives the movement of the buoy in real time from the MCS.
- The robot moves in accordance with the received data and transmits the resistance of the wire connecting the robot and the PTO to the MCS.
- MCS adjusts the resistance of the wire.
- The procedure is then repeated to test a point-absorbed WEC in a lab environment, which could be in another part in the world.

9 Summary of papers

This section briefly presents all papers included in this thesis, and also the author's contributions to each paper.

Paper I

Low-RPM Torque Converter (LRTC)

The paper presents a new WEC concept, the LRTC-WEC. This concept proposal has two rotating generators designed specifically for slow-motion conversion. The LRTC-WEC PTO is placed on the seabed and connected to a buoy at the sea surface. A scale model of the concept was created, the concept was evaluated and validated in a laboratory setting utilizing an industrial 6-DOF ABB robot as test rig.

The author developed the experimental setup, performed the practical experiments, analysed the practical experiment result and wrote part of the experiment and result sections.

Paper published 2021 in *Energies,* vol.14, no.16, 5071.

Paper II

The Low-RPM torque converter (LRTC) with integrated direct shaft flywheel

This article presents an upgrade of the LRTC-WEC concept, investigating a direct flywheel integration to the LRTC-WEC and its effect on the generated output power. Three case experiments are presented in this investigation. The first two experiments investigate the performance of the flywheels and compare the performance of the LRTC-WEC system with and without the flywheels. The third experiment examines the optimization of the flywheel mass. All experiments are performed using the robot dry test rig.

The author developed the experimental setup, performed the practical experiments, analysed the practical experiment result and wrote the paper.

Paper published 2023 in *International Marine Energy Journal*, vol.6, no.1, pp.1–10.

Paper III

A robotized 6-DOF dry test rig for wave power

This paper presents a new robotized 6-DOF dry test rig concept for wave power, evaluates its performance, and validate the concept. A complete robot dry test rig prototype was constructed and evaluated with LRTC-WEC PTO prototype. The assessments confirm significant motion flexibility and accuracy, even when emulating recorded wave and buoy motions.

The author contributed to the conceptual development, developed the experimental setup, performed the practical experiments and contributed to analyzing the practical experiment results.

Paper published 2023 in *Sustainable Energy Technologies and Assessments,* vol.59, 103393.

Paper IV

Demonstrating real-time hydrodynamic motion response in force control for regular waves in a robotized dry test rig with a point-absorber WEC

This paper presents the demonstration and evaluation of the interaction between the robot test rig and the LRTC-WEC PTO under regular wave conditions. A hydrodynamic model with the force control method was used. The sensitivity of the damping response poses a regulatory difficulty, which could affect the stability of the robot.

The author developed the experiment setup, performed the experiments, analysed the experiment result and wrote most of the paper.

Presented by author at the *15th European Wave and Tidal Energy Conference Series (EWTEC2023)*, Bilbao, Spain, September 2023.

Paper V

Evaluating position control for real-time hydrodynamic motion response in a robotized dry test rig with a point-absorber WEC

The present study further investigates the position control method. Focus is on evaluating a control lag in the system, which can cause to an imbalance in specific emulation conditions. A solution for an updated position control method with significantly reduced control lag is presented in robot simulations and compared with hydrodynamic model simulations and actual robot operations for two buoy sizes in regular wave conditions in 1-DOF.

The author developed the experimental setup, performed the practical experiments, analysed the experiment result and wrote most of the paper.

Presented by author at the *43rd International Conference on Ocean, Offshore & Arctic Engineering (OMAE2024),* Singapore, June 2024

Paper VI

A robotized force controlled dry test rig with real-time response hydrodynamic impact evaluated with irregular sea wave motions

This paper evaluates the robot test rig concept in 1-DOF in the heave direction, comparing it to a numerical model based in LPF theory. This experiment used the robot's integrated force control option to simulate a physical PTO. A wave tank experiment was conducted with a two-body WEC and a linear damper PTO, using the data to validate the numerical model the wave tank experiments validated and assessed the numerical model, which was subsequently verified and evaluated the robot test rig against the numerical model.

The author developed the experimental setup, performed the practical robot experiments, analyzed the result of robot experiment and wrote most of the robot part of the paper.

Unpublished Manuscript, December 2024.

Paper VII

Preparing the Uppsala University wave energy converter generator for large-scale production

This article outlines the main design of the UU-WEC PTO. Modifications relating to the material costs of the generator and the potential advantages of automated large-scale production are outlined. The potential for large-scale automated production and assembly is explained for key production steps.

The author contributed to developing tools and experiments.

Presented by Erik Hultman at the *5th International Conference on Ocean Energy*, Halifax, Canada, November 2014.

Paper VIII

Robotized surface mounting of permanent magnets

This paper presents a new robot cell concept for the surface mounting of PMs on the UU-WEC PTO translator. The concept was investigated using the simulation software RobotStudio and validated at full scale in a laboratory environment. The concept reduces monotonous, laborious, and time-consuming manual tasks, also resulting in potential cost savings relative to manual assembly. Further research is necessary for production implementation.

The author developed all robot tools, designed the robot cell, contributed to experiments and to the robot cell validation.

Published in *MDPI Machines*, vol.2, pp.219-232, 2014. In the Special Issue “Advances and Challenges in Manufacturing Automation”.

Paper IX

Robotized manufacturing of rubber components for commercialization of the Uppsala University wave energy converter concept

This paper introduces a robot cell concept for the manufacturing of rubber discs for the UU-WEC PTO. The method was experimentally assessed and validated for the manufacturing of rubber discs. The robot cell replaces monotonous, tiring, and time-consuming tasks, while providing a potential reduction in costs relative to manual work. More development is required for the robot cell to be implemented in a production line.

The author contributed to the design and to the validation of the robot cell. Presented by the Erik Hultman at the *2nd International Conference on Offshore Renewable Energy*, Glasgow, UK, September 2016.

Paper X

Learnings from the rapid online transition of a real-world project task-based engineering course

This study outlines the results and knowledge gained from an accelerated, unexpected transition to distance education for a campus-based, hands-on, lab-intensive robot course. It highlights the combination of an innovative online lecture format with completely online robot laboratory activities. Additionally, practical laboratory exercises and study trips were eliminated from this shift.

The author was responsible for, performed and contributed to the evaluation of the transition of campus-based hands-on laboratory sessions to entirely virtual online simulation labs.

Presented by Erik Hultman at *Frontiers in Education Conference (FIE2022),* Uppsala, October 2022.

Published 2022 in *IEEE Frontiers in Education Conference (FIE)*, pp.1-9

Paper XI

Variable renewable energy sources for powering reverse osmosis desalination, with a case study of wave powered desalination for Kilifi, Kenya

This paper investigates the power supply of desalination using wave energy. Experiments were conducted on a small-scale desalination system in a laboratory setting, with power levels varied throughout the tests. The data from the experiments were combined with resource data from Kilifi, Kenya, and energy production estimates from a WEC to assess the potential for freshwater production at the site. Additionally, a hybrid power supply option is discussed.

The author developed the experimental setup, performed the experiments and contributed with analysing experiment results.

Published 2020 in *Desalination*, vol.494, 114669.

10 Svensk sammanfattning

Runt om i världen forskas och utvecklas teknik för att utnyttja förnybara energikällor i strävan efter ett hållbart och miljövänligt samhälle. Vid Uppsala universitets Avdelning för Elektricitetslära bedrivs forskning om olika förnybara energikällor för elgenerering. Över 40 forskare har disputerat inom vågenergi vid avdelningen, och flera vågenergiomvandlare (WECs) har undersökts.

Ett av de mer kända koncepten som utvecklats är Uppsala universitets vågenergiomvandlare (UU-WEC) som är en linjär vågenergiomvandlare. Konceptet består av två huvudkomponenter; en är generatorn som placeras i havsbotten och andra är en flytboj som placeras på havsytan.

Generatorn består av en tre meter lång magnetklump (translator) som en rörlig del, placerad mitt i höljet och omringad av tre kabellindade sektioner (spole). Translatorn (motsvarande en rotor i en roterande elektrisk maskin), kopplas till bojen på havsytan via en vajer, med vågornas rörelse upp och ned lyfts bojen upp/ned vilket drar med sig translatorn upp och låter den falla ner med gravitationskraften. Med återkommande och upprepande procedur genom att translatorn rör sig upp/ned induceras spänning i spolen.

Ett annat WEC koncept som har tagits fram är LRTC-WEC, som består av två roterande generatorer kopplade mot varandra via en avancerad trumma. Konceptet fungerar på samma sätt som UU-WEC där generatorerna placeras på havsbotten och kopplas till en boj på havsytan.

En viktig del i utvecklingen av WECs är att i tidigt skede kunna testa och utvärdera koncepten. En ytterligare viktig punkt är att kunna automatisera produktionen för att kunna tillverka WECs mer kostnadseffektivt.

Denna avhandling innehåller fyra delprojekt, två stora och två minder projekt.

1. Huvuddelen i denna avhandling handlar om utvecklingen av en robotiserad testrigg för testning och utvärdering av olika WEC koncept.
2. Den andra delen handlar om robotiserad produktion av delar från UU-WEC.
3. Del tre innefattar utveckling av en ingenjörskurs från helt campusbaserad till en online distanskurs, med fokus på virtuella laborationsmoment.
4. I den fjärde och sista delen, undersöks möjligheterna att använda WEC för att driva en avsaltningspark.

Alla WEC koncept måste på något sätt testas och utvärderas. Historisk testas koncepten i havet eller i vågtank vilket är en tidskrävande och dyr process. Så kallade torra testriggar av olika slag har tagits fram världen runt för testning av olika WEC koncept på land. Ofta är testriggar specialbyggda för ett specifikt WEC koncept och verkar i endast en frihetsgrad.

I del ett i denna avhandling utvecklades en torr testrigg med integrerad hydrodynamisk modell. En befintlig 6-axlig industrirobot från ABB används för testning och utvärdering av olika WEC koncept i flera frihetsgrader. Med kraftåterkoppling och implementerad hydrodynamisk modell kan robotens sjätte axel efterlikna (emulera) rörelsen av en boj på havsyta.

Konceptet går ut på att en WEC kan kopplas till robotens sjätte axel för att utvärderas genom teströrelser med olika reguljära och irreguljära vågrörelser med olika bojtyper.

Två olika styrmetoder har utvecklats, en kraft- och en positions-styrd metod. Både metoderna har verifierats och utvärderats.

I den andra delen i denna avhandling, undersöks robotiserad produktion av två delar från UU-WEC. Ett kritisk, svårt, monoton och tidskrävande arbetsmoment är manuell magnetisering av translatorn, som magnetiseras genom montering av 848 stycken Neodym Järn Bor ($Nd_2Fe_{14}B$) magneter av storleken 115 x 47 x 11 mm.

En annan del i produktionen som anses vara ett monotont och riskabelt arbetsmoment är manuell stansning av gummiskivor. Ca 65 gummiskivor används i en UU-WEC, vardera med ytterdiameter 250 mm och innerdiameter 100 mm och tjocklek på 25 mm.

Automatiserade lösningsförslag för både momenten undersöktes och togs fram, inklusive verktyg och robotcellkoncept. Lösningarna verifierades och utvärderades.

Del tre, handlar om pedagogisk utveckling för en kurs i robotteknik som gavs till ingenjörsstudenter. Kursen är helt campusbaserad, och syftar på djup inlärning genom en kombination av föreläsningar, projekt och laborationer med industriella 6-axliga robotar i våra labbsalar. På grund av utbrottet av COVID-19, var vi som många andra i världen, tvungna att övergå till helt online distansutbildning. Inom kort fick alla fysiska laborationer på kursen ersättas med inspelad video och simuleringsbaserade projekt.

Examinationsresultat och kursvärderingar visar på en lyckad omformning av kursen, som fortfarande fyller sitt syfte relaterat till kurskriterier.

En mindre del i avhandlingen handlar om möjligheten att driva en avsaltningspark med förnybara energikällor. Att WEC och avsaltningspark befinner sig i direkt koppling till varandra, gör att undersökningen är av mer intresse. En mindre experimentuppsättning undersöktes i labbmiljö. Saltvatten från en tank pumpades genom en avsaltningsenhet med olika tryck, vilket gav sötvatten med olika kvalitetsnivåer.

Syftet var att undersöka effektåtgången hos enheten för olika vattenkvalitetsnivåer. Resultatet från experimenten togs vidare för undersökning och utvärdering för potentialen att använda WEC för avsaltning.

11 Acknowledgements

To begin with, I want to thank professor Mats Leijon, for giving me the opportunity to do my PhD and trusting me to work freely all the way through several projects.

A special thanks to my supervisor and officemate Erik Hultman for both supervision and all the fruitful conversations we shared in the office over the years. He has significantly aided in my personal and scientific growth. I also want to thank Antoine Dupuis for all the help, support, valuable conversations, and enjoyable times. I would like to thank the entire Division for Electricity for all the support and fun times we had over the years, both at the Division and at conferences around the world.

The author is thankful to ABB Corporate Research, ABB Robotics, and the Swedish STandUP for Energy and the Swedish Research Council for supporting the presented work, and Uppsala University for funding the presented work.

12 References

[1] Junejo, F., Saeed, A. and Hameed, S. (2018) Energy Management in Ocean Energy Systems. Comprehensive Energy Systems, vol.5, pp.778-807, https://doi.org/10.1016/B978-0-12-809597-3.00539-3.

[2] Falnes, J. (2002) Ocean Waves and Oscillating Systems: Linear Interactions Including Wave-Energy Extraction. Cambridge: Cambridge University Press.

[3] Mueller, M. and Wallace, R. (2008), Enabling science and technology for marine renewable energy, Energy Policy, vol.36, no.12, pp.4376-4382

[4] Elwood, D., C. Yim, S., Prudell, J., Stillinger, C., von Jouanne, A., Brekken, T., Brown, A. and Paasch, R. (2010) Design, construction, and ocean testing of a taut-moored dual-body wave energy converter with a linear generator power take-off. Renewable Energy, vol.35, pp.348−354.

[5] Dongsheng, Q., Rizwan, H., Jun, Y., Dezhi, N., Binbin, L. (2020) Review of Wave energy converter and design of mooring System. Sustainability, vol.12, no.19, 8251.

[6] Thorburn, K. (2006) Electric energy conversion systems: Wave Energy and Hydropower, PhD thesis, Uppsala University.

[7] Danielsson, O. (2006) Wave energy conversion - Linear synchronous permanent magnet generator, PhD thesis, Uppsala University.

[8] Eriksson, M. (2007) Modelling and experimental verification of direct drive wave energy conversion, PhD thesis, Uppsala University.

[9] Waters, R. (2008) Energy from ocean waves, PhD thesis, Uppsala University.

[10] Langhamer, O. (2009) Wave energy conversion and the marine environment PhD thesis, Uppsala University.

[11] Rahm, M. (2010) Ocean wave energy - Underwater substation system for wave energy converters, PhD thesis, Uppsala University.

[12] Boström, C. (2011) Electrical systems for wave energy conversion, PhD thesis, Uppsala University.

[13] Engström, J. (2011) Hydrodynamic modelling for a point absorbing wave energy converter, PhD thesis, Uppsala University.

[14] Simon, L. (2011) Buoy and generator interaction with ocean waves - Studies of a wave energy conversion system, PhD thesis, Uppsala University.

[15] Savin, A. (2012) Experimental measurement of lateral force in a submerged single heaving buoy wave energy converter, PhD thesis, Uppsala University.

[16] Strömstedt, E. (2012) Submerged transmission in wave energy converters - Full scale in-situ experimental measurements, PhD thesis, Uppsala University.

[17] Svensson O. (2012) Experimental results from the Lysekil wave power research site, PhD thesis, Uppsala University.

[18] Ekergård, B. (2013) Full scale applications of permanent magnet electromagnetic energy converters - From Nd2Fe14B to Ferrite, , PhD thesis, Uppsala University.
[19] Ekström, E. (2014) Offshore marine substation for grid-connection of wave power farms: An experimental approach, , PhD thesis Uppsala University.
[20] Gravråkmo, H. (2014) Buoy geometry, size and hydrodynamics for power take off device for point absorber linear wave energy converter, PhD thesis, Uppsala University.
[21] Haikonen, K. (2014) Underwater radiated noise from point absorbing wave energy converters, PhD thesis, Uppsala University.
[22] Krishna, R. (2014) Grid connected three-level converters - Studies for wave energy conversion, , PhD thesis, Uppsala University.
[23] Hai, L. (2015) Modelling Wave Power by Equivalent Circuit Theory, PhD thesis, Uppsala University.
[24] Apelfröjd, S. (2016) Grid Connection of permanent magnet generator based renewable energy systems PhD thesis, Uppsala University.
[25] Castellucci, V. (2016) Sea level compensation system for wave energy converters PhD thesis, Uppsala University.
[26] Hong, Y. (2016) Numerical modelling and mechanical studies on a point absorber type wave energy converter PhD thesis, Uppsala University.
[27] Lejerskog, E. (2016) Theoretical and experimental analysis of operational wave energy converters PhD thesis, Uppsala University.
[28] Li, W. (2016) Numerical modelling and statistical analysis of ocean wave energy converters and wave climates PhD thesis, Uppsala University.
[29] Sjökvist, S (2016) Demagnetization and fault simulations of permanent magnet generators PhD thesis, Uppsala University.
[30] Baudoin, A. (2016) Cooling strategies for wave power conversion systems PhD thesis, Uppsala University.
[31] Soman, D. E. (2017) Multilevel power converters with smart control for wave energy conversion PhD thesis, Uppsala University.
[32] Kamf, T. (2017) Automated production technologies and measurement systems for ferrite magnetized linear generators PhD thesis, Uppsala University.
[33] Sjökvist, L. (2017) Wave loads and peak forces on moored wave energy devices in tsunamis and extreme waves PhD thesis, Uppsala University.
[34] Ulvgård, L. (2017) Wave energy converters - an experimental approach to onshore testing, deployments and offshore monitoring PhD thesis, Uppsala University.
[35] Wang, L. (2017) Modelling and advanced control of fully coupled wave energy converters subject to constraints: the Wave-to-wire approach PhD thesis, Uppsala University.
[36] Hultman, E. (2018) Robotized production methods for special electric machines PhD thesis, Uppsala University.
[37] Remouit, F. (2018) Automation of underwater operations on wave energy converters using remotely operated vehicles PhD thesis, Uppsala University.
[38] Forslund, J. (2018) Studies of a vertical axis turbine for marine current energy conversion - Electrical system and turbine performance PhD thesis, Uppsala University.
[39] Ayob, N. (2019) Adaptation of wave power plants to regions with high tides PhD thesis, Uppsala University.
[40] Parwal, A. (2019) Grid integration and impact of a wave power system PhD thesis, Uppsala University.

[41] Chatzigiannakou, M. A. (2019) Offshore deployments of marine energy converters PhD thesis, Uppsala University.
[42] Leijon, J. (2020) Wave power for desalination PhD thesis, Uppsala University.
[43] Giassi, M. (2020) Numerical and experimental modelling for wave energy arrays optimization PhD thesis, Uppsala University.
[44] Frost, A. E. (2021) In the air gap of linear generators for wave power PhD thesis, Uppsala University.
[45] Bender, A. (2022) Environmental effects from wave power: Artificial reefs and incidental no-take zones PhD thesis, Uppsala University.
[46] Potapenko, T. (2022) Modelling of ocean wave energy conversion for increased power absorption PhD thesis, Uppsala University.
[47] Katsidoniotaki, E. (2023) Offshore renewable energy systems: Quantification of extreme loads using computational methods PhD thesis, Uppsala University.
[48] Shahroozi, Z. (2024) Survivability control using data-driven approaches and reliability analysis for wave energy converters PhD thesis, Uppsala University.
[49] Fjellstedt, C. (2024) Studies of the grid connection of offshore renewable energy sources: technologies and simulations PhD thesis, Uppsala University.
[50] Leijon, M., Bernhoff, H., Ågren, O., Isberg, J., Sundberg, J., Berg, M., Karlsson, K.E., and Wolfbrandt, A. (2005) Multiphysics simulation of wave energy to electric energy conversion by permanent magnet linear generator, IEEE transactions of energy conversion, vol.20, no.1, pp.219–224.
[51] Leijon, M., Boström, C., Danielsson, D., Gustafsson, S., Haikonen, K., Langhamer, O., Stromstedt, E., Stålberg, M., Sundberg, J., Svensson, O., Tyrberg, S. and Waters, R. (2008) Wave energy from the North Sea: Experiences from the Lysekil research site. Surveys in Geophysics, vol.29, pp.221−240.
[52] Leijon, M., Waters, R., Rahm, M., Svensson, O., Boström, C., Strömstedt, E., Engstrom, J., Tyrberg, S., Savin, A., Gravrakmo, H., Bernhoff, H., Sundberg, J., Isberg, J., Agren, O., Danielsson, O., Eriksson, M., Lejerskog, E., Bolund, B., Gustafsson, S. and Thorburn, K. (2009) Catch the wave to electricity. IEEE Power and Energy Magazine, vol.7, Issue 1, pp.50–54.
[53] Lejerskog, E., Bostrom, C., Hai, L., Waters, R., Leijon, M. (2015) Experimental results on power absorption from a wave energy converter at the Lysekil wave energy research site. Renew Energy vol.77, pp.9–14. https://doi.org/10.1016/j.renene.2014.11.050
[54] Samad, A., Kumar, P., Kumar, S., Singh, D., Kapse, S., Hossain, S., Chakarvarthi, TK., Paul, AR., Chaudhuri, A., Chattopadhaya, S. and Arun Kiran Karthik, S.S. (2023) Open sea trial of a wave-energy converter at tuticorin port – Challenges, EWTEC 15. https://doi.org/10.36688/ewtec-2023-484
[55] Xiangnan, W., Hainan, X., Yi, G., Yunqi, D., Meng, W., Yuzheng, L. and Huimin, S. (2023) Research on field testing and assessment technology of ocean energy converters, Ocean Engineering vol.285, no.2, 115539. https://doi.org/10.1016/j.oceaneng.2023.115539
[56] Bacelli, G., Spencer, S.J., Patterson, D.C. and Coe, R.G. (2019) Wave tank and bench-top control testing of a wave energy converter, Applied Ocean Research, vol.86, pp.351-366. https://doi.org/10.1016/j.apor.2018.09.009
[57] Falcão, A.F.O. and Henriques, J.C.C. (2014) Model-prototype similarity of oscillating-water-column wave energy converters, Int J of Marine Energy vol.6 pp.18-34. http://dx.doi.org/10.1016/j.ijome.2014.05.002

[58] Berque, J., Zarate, I., Blanco, J., Bidaguren, I., Touzon , I. and Fernández, L. (2023) A new type of wave tank: prototype and proof of concept . Proceedings of the European Wave and Tidal Energy Conference. 15, https://doi.org/10.36688/ewtec-2023-276

[59] Wahyudie, A., Jama, M., Susilo, T.B., Mon, B.F., Shaaref, H. and Noura, H. (2017) Design and testing of a laboratory scale test rig for wave energy converters using a double-sided permanent magnet linear generator, IET Renew Power Gener vol.11, no.7, pp.922–30. https://doi.org/10.1049/iet-rpg.2016.0874

[60] Baker, NJ., Mueller, MA., Ran, L., Tavner, PJ. and McDonald, S. (2007) Development of a linear test rig for electrical power take off from waves. J of Marine Eng & Technology, vol.6, no.2, pp.3–15. https://doi.org/10.1080/20464177.2007.11020201.

[61] De Koker, KL., Crevecoeur, G., Meersman, B., Vantorre, M. and Vandevelde, L. (2016) A wave emulator for ocean wave energy, a Froude-scaled dry power take-off test setup. Renew Energy vol.105, pp.712–21. https://doi.org/10.1016/j.renene.2016.12.080

[62] Bracco, G., Giorcelli, E., Mattiazzo, G., Orlando, V. and Raffero, M. (2015) Hardware-in-the-loop test rig for the ISWEC wave energy system. Mechatronics, vol.25, pp.11-17. http://dx.doi.org/10.1016/j.mechatronics.2014.10.007

[63] Imai, Y., Nagata, S., Murakami, T. and Chen, DW. (2016) Design of a hydraulic power take-off test rig for wave energy converters. Proceedings of the Techno-Ocean Conference, Kobe, Japan. https://ieeexplore.ieee.org/document/7890708

[64] Chae, Y., Kazemibidokhti, K. and Ricles, JM. (2013) Adaptive time series compensator for delay compensation of servo–hydraulic actuator systems for real–time hybrid simulation. Earthquake Eng Struct Dyn, vol.42, pp.1697–715. https://doi.org/10.1002/eqe.2294

[65] Ha, Y.-J., Park, J.-Y., Kim, K.-H., Won, Y.U., Oh, Y.J. and Lee, J.H. (2023) An experimental study for wave energy converter of wavestar type using real-time hybrid model testing technique. Proceedings of the European Wave and Tidal Energy Conference. 15. https://doi.org/10.36688/ewtec-2023-152

[66] Hals Todalshaug, J., Ásgeirsson, G.S., Hjálmarsson, E., Maillet, J., Möller, P., Pires, P., Guérinel, M. and Lopes, M. (2016) Tank testing of an inherently phase-controlled wave energy converter, International Journal of Marine Energy, vol.15, pp.68-84, ISSN 2214-1669, https://doi.org/10.1016/j.ijome.2016.04.007

[67] Froude, W. (2022) Observations and suggestions on the subject of determining by experiment the resistance of ships, in: The Papers of William Froude, Transactions INA, 1955, pp. 1810e1879.

[68] Vassalos, D. (1998) Physical modelling and similitude of marine structures, Ocean Engineer, vol.26, no.2, pp.111-123, http://dx.doi.org/10.1016/S0029-8018(97) 10004-X.

[69] Hernández-Robles, A.I., González-Ramírez, X., Gómez-Gutiérrez, J.A. and Ramirez, J.M. (2021) Wave power assessment for electricity generation with powerbouy system by wave motion emulation modelling, Sustainable Energy Technologies and Assessments, vol.43, 100962, ISSN 2213-1388, https://doi.org/10.1016/j.seta.2020.100962.

[70] De Koker, K., Crevecoeur, G., Meersman, B., Vantorre M. and Vandevelde L. (2017) A wave emulator for ocean wave energy, a Froude-scaled dry

power take-off test setup, Renewable Energy, vol.105, pp.712-721, ISSN 0960-1481, https://doi.org/10.1016/j.renene.2016.12.080.
[71] Eriksson, M., Isberg, J. and Leijon, M. (2005) Hydrodynamic modelling of a direct drive wave energy converter. International Journal of Engineering Science 43, 1377-1387.
[72] Lee, C. and Newman, J.N. (2013) Wamit–user manual version 7.0. WAMIT Inc, Chestnut Hill, Massachusetts.
[73] Falnes , J. and Kurniawan, A. (2020) Ocean waves and oscillating systems: linear interactions including wave-energy extraction, vol.8. Cambridge university press.
[74] Eriksson, M., Waters, R., Svensson, O., Isberg, J. and Leijon, M. (2007) Wave power absorption: Experiments in open sea and simulation. Journal of Applied Physics, vol.102, no.8.
[75] COAST. Coast laboratory facilities. https://www.plymouth.ac.uk/ facilities/coast-laboratory/facilities. Accessed: April 22, 2024.
[76] Obal, P., Gierlak, P. (2021) EGM Toolbox—Interface for Controlling ABB Robots in Simulink. Sensors, vol.21, 7463. https://doi.org/10.3390/ s21227463
[77] Dupuis, A., Shahroozi, Z. and Engström, J. (2024) Experimental study and surrogate modeling of a scaled eddy current power-take-off. In Developments in Renewable Energies Offshore. CRC Press, pp.473-482.
[78] Hultman, E. and Leijon, M. (2013) Utilizing cable winding and industrial robots to facilitate the manufacturing of electric machines. Robot. Comput. Integr. Manuf, vol.29, pp.246-256.
[79] Hultman, E., Ekergård, B. and Leijon, M. (2012) Electromagnetic, mechanical and manufacturing properties for cable wound direct-drive PM linear generators for offshore environments. Presented at the 31st International Conference on Ocean, Offshore and Arctic Engineering, Rio de Janeiro, Brazil.
[80] Hong, Y., Eriksson, M., Boström, C. and Waters, R. (2016) Impact of generator stroke length on energy production for a direct drive wave energy converter. Energies, vol.9, no.730. https://doi.org/10.3390/en9090730
[81] Haring, T., Forsman, K., Huhtanen, T. and Zawadzki, M. (2003) Direct drive – opening a new era in many applications. In: Conference Record of the Annual Pulp and Paper Industry Technical Conference. Charleston, USA, pp. 171-179.
[82] Hsieh, MF., Hsu, YC. and Dorrell, DG. (2010) Design of large-power surface-mounted permanent-magnet motors using post-assembly magnetization. IEEE Transactions on Industrial Electronics, vol.57, pp.3376-3384.
[83] Aleksashkin, A. and Mikkola, A. (2008) Literature review on permanent magnet generators design and dynamic behavior. Research Report 77. Lappeenranta University of Technology: Lappeenranta, Finland.
[84] Binder, A., Schneider, T. and Klohr, M. (2006) Fixation of buried and surface-mounted magnets in high-speed permanent-magnet synchronous machines. IEEE Transactions on Industrial Applications, vol.42, pp.1031-1037.
[85] Franke, J., Tremel, J. and Kühl, A. (2011) Innovative developments for automated magnet handling and bonding of rare earth magnets. In: Proceedings of the IEEE International Symposium on Assembly and Manufacturing. Tampere, Finland, pp.1-5.
[86] Joseph, E., Tremel, J., Hofmann, B., Meyer, A., Franke, J. and Eschrich, S. (2013) Automated magnet assembly for large PM synchronous machines

with integrated permanent magnets. In: Proceedings of the 3rd International Electric Drives Production Conference. Nuremberg, Germany, pp.1-6.
[87] Tremel, .J, Hofmann, B. and Risch, F. (2013) Handling and fixation of permanent magnets. Advanced Material Research, vol.769, pp.3-10.
[88] Karim, A. and Verl, A. (2013) Challenges and obstacles in robot-machining. In: Proceedings of the 44th International Symposium on Robotics. Seoul, South Korea.
[89] Sörnmo, O., Olofsson, B., Schneider, U., Robertsson, A. and Johansson, R. (2012) Increasing the milling accuracy for industrial robots using a piezo-actuated high-dynamic micro manipulator. In: Proceedings of the International Conference on Advanced Intelligent Mechatronics. Kaohsiung, Taiwan.
[90] Atmosudiro, A., Keiner,t M., Karim, A., Lechler, A., Verl, A. and Csizar, A. (2014) Productivity increaser through joint space path planning for robot machining. In: Proceedings of the 8th European Modelling Symposium. Pisa, Italy.
[91] Wang, J., Zhang, H. and Fuhlbrigge, T. (2009) Improving machining accuracy with robot deformation compensation. In: Proceedings of the International Conference on Intelligent Robots and Systems. St. Louis, USA.
[92] Domrös, F., Riege,r M. and Kuhlenkötter, B. (2014) Towards autonomous robot machining. In: Proceedings of the 41st Int. Symposium on Robotics. Munich, Germany.
[93] De Graaf, E. and Ravensteijn, W. (2010) Training complete engineers: global enterprise and engineering education. European Journal of Engineering Education, vol.26, no.4, pp.417-427.
[94] Hanning, A., Abelsson, A.P., Lundqvist, U. and Svanström, M. (2012) Are we educating engineers for sustainability?" International Journal of Sustainability, vol.13, no.3, pp.305-320.
[95] Duderstadt, J.J. (2008) Engineering for a changing world: A roadmap to the future of engineering practice, research and education, Springer, New York.
[96] Zhou, C. (2012) Fostering creative engineers: a key to face the complexity of engineering practice. European Journal of Engineering Education, vol.37, no.4, pp.343-353.
[97] Beder, S. (1999) Beyond technicalities: Expanding engineering thinking. Journal of Pro-fessional Issues in Engineering Education and Practice, vol.125, no.1, pp.12-18.
[98] Cruickshank, HJ. and Fenner, RA. (2007) The evolving role of engineers: towards sustainable development of the built environment. Journal of International Development, vol.19, pp.111-121.
[99] Duderstadt, JJ. (2008) Engineering for a changing world: a roadmap to the future of engineering practice, research and education. Ann Arbor: University of Michigan.
[100] Rugarcia A, Felder RM, and Woods DR. (2000)The future of engineering education I: a vision for a new century. Chemical Engineering Education, vol.34, no.1, pp.16-25.
[101] Dhawan, S. (2020) Online learning: a panacea in the time of COVID-19 crisis, Journal of Education Technology Systems, vol.49, no.1, pp.5-22.
[102] O.B. Adedoyin, E. Soykan, "Covid-19 pandemic and online learning: the challenges and opportunities," Interactive Learning Environments, vol. 2, no.1, pp. 1-13, 2020.

[103] Grodotzki, J., Upadhya, S. and Tekkaya, A.E. (2021) Engineering education amid a global pandemic, Advances in Industrial and Manufacturing Engineering, vol.3, 100058.
[104] United Nations, (2017) Factsheet: People and Oceans," in The Ocean Conference.
[105] Mekonnen, M.M. and Hoekstra, A.Y. (2016) Four billion people facing severewater scarcity, Sci. Adv., vol.2, no.2, pp.1–6. doi:10.1126/scadv.1500323
[106] Abdelkareem, M.A., El Haj Assad, M., Sayed, E. T. and Soudan, B. (2017) Rcentprogress in the use of renewable energy sources to power water desalination plants, Desalination, vol.435, pp.97–113. doi: 10.1016/j.desal.2017.11.018.
[107] Ghaffour, N., Bundschuh, J., Mahmoudi, H. and Goosen, M. F. A. (2015) Renewable energy-driven desalination technologies: A comprehensive review on challenges and potential applications of integrated systems, Desalination, vol.356, pp.94–114. doi: 10.1016/j.desal.2014.10.024.
[108] Sharon, H. and Reddy, K. S. (2014) A review of solar energy driven desalination technologies," Renew. Sustain. Energy Rev., vol.41, pp.1080–1118. doi: 10.1016/j.rser.2014.09.002.
[109] Ali, R., Tufa, A., Macedonio, F., Curcio, E. and Drioli, E. (2018) Membrane technology in renewable-energy-driven desalination," Renew. Sustain. Energy Rev., vol.81, pp.1–21. doi: 10.1016/j.rser.2017.07.047.
[110] Loutatidou, S., Liosis, N., Pohl, R., Ouarda, T. B. M. J. and Arafat, H. A. (2017) Wind-powered desalination for strategic water storage: Techno-economic assessment of concept, Desalination, vol.408, pp.36–51. doi: 10.1016/j.desal.2017.01.002.
[111] Folley, M. and Whittaker, T. (2009) The cost of water from an autonomous wave-powered desalination plant, Renew. Energy, vol.34, pp.75–81. doi: 10.1016/j.renene.2008.03.009.
[112] Ozcelik, M. (2017) Alternative model for electricity and water supply after disaster, J. Taibah Univ. Sci., vol.11, no.6, pp.966–974. doi: 10.1016/j.jtusci.2017.01.002.

Acta Universitatis Upsaliensis

Digital Comprehensive Summaries of Uppsala Dissertations from the Faculty of Science and Technology 2485

Editor: The Dean of the Faculty of Science and Technology

A doctoral dissertation from the Faculty of Science and Technology, Uppsala University, is usually a summary of a number of papers. A few copies of the complete dissertation are kept at major Swedish research libraries, while the summary alone is distributed internationally through the series Digital Comprehensive Summaries of Uppsala Dissertations from the Faculty of Science and Technology. (Prior to January, 2005, the series was published under the title "Comprehensive Summaries of Uppsala Dissertations from the Faculty of Science and Technology".)

Distribution: publications.uu.se
urn:nbn:se:uu:diva-544285

ACTA UNIVERSITATIS
UPSALIENSIS
2025